ČESKÉ VYSOKÉ UČENÍ TECHNICKÉ V PRAZE
Fakulta jaderná a fyzikálně inženýrská

BAKALÁŘSKÁ PRÁCE

2012 KarolJeško

ČESKÉ VYSOKÉ UČENÍ TECHNICKÉ V PRAZE
Fakulta jaderná a fyzikálně inženýrská
Katedra fyziky

BAKALÁŘSKÁ PRÁCE

Okrajové plazma v tokamacích a jeho diagnostika

Edge plasma in tokamaks and its diagnostics

Posluchač: Karol Ješko
Školitel: Ing. Ivan Ďuran, Ph.D.
Akademický rok: 2011/2012

Na toto místo přijde svázat **Zadání bakalářské práce**!
V jednom z výtisků musí být **originál** zadání, v ostatních kopie.

Čestné prohlášení

Prohlašuji na tomto místě, že jsem předloženou práci vypracoval samostatně a že jsem uvedl veškerou použitou literaturu.

Nemám závažný důvod proti užití tohto školního díla ve smyslu §60 Zákona č. 121/2000 Sb., o právu autorském, o právech souvisejících s právem autorským a o změně některerých zákonů (autorský zákon).

V Praze dne 8. července 2012 ....

Jméno Příjmení

Poděkování

Děkuji Ing. Ivanovi Ďuranovi, Ph.D. za vedení mé bakalářské práce a za podnětné návrhy, které ji obohatily.

Karol Ješko

Název práce: **Okrajové plazma v tokamacích a jeho diagnostika**

Autor: Karol Ješko

Obor: Fyzikální inženýrství

Zaměření: Fyzika a technika termojaderné fúze

Druh práce: Bakalářská práce

Vedoucí práce: Ing. Ivan Ďuran, Ph.D., Ústav fyziky plazmatu AV ČR, v. v. i.

Abstrakt: Táto práca popisuje základné pojmy fyziky plazmy a základné princípy fungovania tokamakov, s dôrazom na javy vyskytujúce sa v okrajovej vrstve týchto zariadení. Pochopenie zákonistostí týchto javov je dôležité pre budúce komerčné využitie tokamakov ako fúznych reaktorov. Pretože horúca okrajová plazma je v kontakte so stenami vákuovej nádoby, a najmä s divertorom, práca obsahuje aj popis diagnostických metód na meranie parametrov tejto plazmy. Finálna časť je venovaná popisu a výsledkom kinetického modelu, ktorý simuluje merania Langmuirovými sondami tesne pri divertore. Pomocou simulácie sa analyzuje časté experimentálne nadhodnocovanie elektrónovej teploty T_e týmito sondami a jeho možné dôvody. Výsledkom simulácií je nadhodnotenie T_e pri špecifických podmienkach panujúcich v okrajovej plazme.

Klíčová slova: Tokamak, Scrape-off layer, Divertor, Langmuirova sonda, Elektrónová teplota

Title: **Edge plasma in tokamaks and its diagnostics**

Author: Karol Ješko

Abstract: In this thesis, basic concepts of plasma physics and the main principles of operation of tokamaks, with emphasis on phenomena that occur in the boundary layer of these magnetic confinement devices are described. The understanding of the laws of these phenomena is essential for future commercial use of tokamaks as fusion reactors. The hot edge plasma in the boundary layer is in contact with the walls of the vacuum vessel, in particular with the divertor plates. Consequently, diagnostic methods used for measuring edge plasma parameters are described. Finally, a simple kinetic model simulating divertor target Langmuir probe measurements is introduced. With the help of the simulation, frequently reported overestimation of T_e measurements by probes and its possible causes will be analysed. The simulations yield overestimation of the electron temperature T_e for specific conditions in the edge plasma.

Key words: Tokamak, Scrape-off layer, Divertor, Langmuir probe, Electron temperature

Contents

1 Introduction to plasma physics **9**
1.1 Plasma definition . . . 9
1.2 The Maxwellian velocity distribution . . . 9
1.3 Debye shielding . . . 10
1.4 Larmor orbits . . . 12

2 Tokamaks **14**
2.1 Magnetic fields . . . 14
2.2 Energy confinement . . . 16
2.3 Heating . . . 17
2.3.1 Ohmic heating . . . 18
2.3.2 Neutral beam injection . . . 18
2.3.3 Radio frequency heating . . . 18
2.4 Tokamak experiments . . . 18
2.4.1 TCV . . . 18
2.4.2 JET . . . 19

3 Edge plasma **21**
3.1 Scrape-off layer, SOL . . . 21
3.2 Limiters . . . 22
3.3 Divertors . . . 23
3.4 Transport in the SOL . . . 24
3.5 The divertor SOL . . . 25
3.6 The plasma sheath . . . 27
3.7 Recycling . . . 28

4 Edge diagnostics **30**
4.1 Langmuir probes . . . 30
4.1.1 Single probes . . . 32
4.1.2 Double probes . . . 32
4.1.3 Triple probes . . . 32
4.1.4 Langmuir probe disadvantages . . . 33
4.2 Other diagnostic methods . . . 35
4.2.1 Thomson scattering . . . 35
4.2.2 Bolometry . . . 35
4.2.3 Infrared thermography . . . 36

5 Analysis of Langmuir probe T_e measurements **38**
5.1 Background 38
5.2 PIC simulations 38
5.3 Simple kinetic model 39
5.3.1 Input data 39
5.3.2 EVDF construction 41
5.3.3 IV characteristic construction 42
5.3.4 Choice of mean free path 43
5.3.5 Model results 44

Conclusion **47**
Summary of the thesis 48
Future plans 49

Chapter 1

Introduction to plasma physics

1.1 Plasma definition

A plasma[1] is matter in the form of an ionized gas, which is a gas whose atoms are separated into ions and electrons. Admittedly, not every ionized gas can be considered a plasma. F. F. Chen [1] uses the following definition:
A plasma is a quasi-neutral gas of charged particles, which exhibits collective behavior.
Quasi-neutral means, that the number of positive charges is very nearly equal to the number of negative charges. The electric charge density of the two types of particles is so large that any significant separation would lead to a very large restoring force, and as a consequence the ion and electron charge densities are almost equal. Collective behaviour means, that the state of the plasma in regions somewhat distant from the point of interest may affect the behavior. The two components, i. e. the electrons and ions have many of the properties of a normal gas. Primarily, they can be described by their particle density and temperature.

1.2 The Maxwellian velocity distribution

In order to describe plasma, it is important to introduce the concept of temperature. To achieve this, we choose a statistical approach. When a set of identical gas or plasma particles is left alone to interact only with each other, collisionally – with no outer forces being present and with no particles entering nor leaving the system, then after a sufficient amount of time a steady state called *thermodynamic equilibrium* results from this self-collisionality. In every point $\mathbf{r} = (x, y, z)$ of the gas, this steady state is characterized by a Maxwellian velocity distribution $f(\mathbf{v})$ of the form

$$f(\mathbf{v}) = f(v_x, v_y, v_z) = C \exp\left(-\frac{bm}{2}\left((v_x - v_{0x})^2 + (v_y - v_{0y})^2 + (v_z - v_{0z})^2\right)\right), \qquad (1.1)$$

where $v_{0x}, v_{0y}, v_{0z}, b, C$ are constants whose physical meaning will be identified below, m is the mass of each particle and $f(v)\mathrm{d}v_x\mathrm{d}v_y\mathrm{d}v_z$ is the number of particles with velocity in $[v_x + \mathrm{d}v_x, v_y + \mathrm{d}v_y, v_z + \mathrm{d}v_z]$ $\mathbf{v} = (v_x, v_y, v_z)$, $\mathrm{d}v = \mathrm{d}v_x\mathrm{d}v_y\mathrm{d}v_z$. All velocities are possible, i.e. $\mathbf{v} \in \mathbf{R}^3$. The Maxwellian velocity distribution function can be derived in several ways, the most common being the derivation from the condition of maximal enthropy of the

[1] The word plasma comes from the Greek "plasmos", meaning adapted, made up.

system[2]. When any of $v_{0x}, v_{0y}, v_{0z} \neq 0$, we have the drifting Maxwellian distribution, with drift or mean velocity $\langle \mathbf{v} \rangle = (v_{0x}, v_{0y}, v_{0z})$. Further on, no drift will be included, that is $\langle \mathbf{v} \rangle = (0, 0, 0)$.
We may transform expression 1.1 to spherical coordinates. In these coordinates, the radial component of the velocity vector is the particle speed:

$$\mathbf{v} = \sqrt{v_x^2 + v_y^2 + v_z^2}, \quad v \in [\,0, +\infty) \tag{1.2}$$

The spherical transformation yields:

$$f(v) = 4\pi v^2 C \exp\Big(-\frac{bm}{2} v^2 \Big) \tag{1.3}$$

Note that this distribution is a function of only one variable. We require that

$$\int_0^\infty f(v)\,\mathrm{d}v = n, \tag{1.4}$$

where n is the number of particles in one m^{-3}, as a normalization. By using standard formulae for Gaussian integrals [3], it can be shown that constants b and C are related by $C = n(\frac{mb}{2\pi})^{3/2}$.
Finally, we may define the temperature of a gas or plasma in convenient way, being proportional to the mean kinetic energy of the system, by satisfying the equation:

$$\frac{3}{2} nkT = n\langle E \rangle = n\Big\langle \frac{1}{2} mv^2 \Big\rangle = \int_0^\infty \frac{1}{2} mv^2 f(v)\,\mathrm{d}v, \tag{1.5}$$

where k is the Boltzmann constant, which is required to ensure compatibility of this definition and the standard, but physically less obvious definition based on the freezing point of water at atmospheric pressure being 273.15 K. From equation 1.5:

$$\Big\langle \frac{1}{2} mv^2 \Big\rangle = \frac{3}{2} kT. \tag{1.6}$$

Due to the close relation of T and $\langle E \rangle$, in plasma physics, it is very common to denote temperature in energy units, mainly eV. To avoid problems with the number of degrees of freedom, not 1.6 is used to determine the temperature. The energy corresponding to kT is used instead. For example, if $kT = 1$ eV $=1.6\times10^{-19}$ J, then

$$T = \frac{1.6 \times 10^{-19}}{1.38 \times 10^{-23}} \mathrm{K} = 11600\mathrm{K}. \tag{1.7}$$

Claiming the plasma temperature to be 2 eV, we mean that $kT = 2$ eV and assuming three degrees of freedom $\langle E \rangle = \frac{3}{2} kT$ =3 eV.

1.3 Debye shielding

As mentioned in section 1.1., the electric charge density of the separate ion and electron components of a plasma is large enough to ensure that only small charge separations occur. The strength of this effect can be acknowledged by imagining the separation of the ions and

[2]The original derivation by J. C. Maxwell assumed that all three directions would behave in the same manner, but a later derivation by L. Boltzmann dropped this assumption by using kinetic theory.

electrons into sheets of thickness d. The system can now be regarded as a capacitor. If the density of both electrons and ions is n, the surface charge density in each of the separated sheets is $\sigma = dne$. The electric field present between the sheets is $E = \frac{\sigma}{\epsilon_0}$. A fundamental length characterizing the plasma can be derived by calculating the maximum thickness d for which the thermal energy of one electron could be equal to the energy needed to move a distance d against the capacitors electric field:

$$eEd = \frac{e^2nd^2}{\epsilon_0} = kT \tag{1.8}$$

By solving this equation, we obtain the *Debye length*:

$$d = \lambda_D = \left(\frac{\epsilon_0 T}{ne^2}\right)^{1/2} \tag{1.9}$$

Despite that the charge separation described above is energetically possible, it can never occur, as particle velocities are random and it is effectively impossible that the imagined displacement arises.
A situation in which a significant charge separation does occur is when a plasma is in contact with a solid surface. Separation can then be observed in a sheath close to the surface, while the thickness of this sheath is λ_D. The Debye length also arises inside the plasma, characterizing the phenomenon called *Debye shielding*[3]. Consider a stationary single-charged ion in the plasma. The magnitude of the electric field of this ion is

$$E = \frac{e}{4\pi\epsilon_0 r^2} \tag{1.10}$$

Although this is the field directly associated with this ion, the other particles in the plasma adjust to this field, changing it in a way that shields the charge of the ion. The shielding occurs around every ion and the reverse effect occurs for every electron. The form of the shielding for a stationary ion can be calculated from Poisson's equation for the potential ϕ. The equation in spherical coordinates has the form

$$\frac{1}{r^2}\frac{\mathrm{d}}{\mathrm{d}r}\left(r^2\frac{\mathrm{d}\phi}{\mathrm{d}r}\right) = -\rho, \tag{1.11}$$

where the charge density for singly charged ions $\rho = n_e(-e) + n_i e$. If the temperature is much higher than the Fermi temperature, then the ions and electrons will each follow a Maxwell-Boltzmann statistic in the potential [1], their densities given by

$$n_j = n_0 \exp\left(-\frac{e\phi}{kT}\right) \tag{1.12}$$

while n_0 is the ion density at a large distance from the chosen ion, where the potential is assumed to be zero. Using 1.12 in 1.11 we obtain:

$$\frac{1}{r^2}\frac{\mathrm{d}}{\mathrm{d}r}\left(r^2\frac{\mathrm{d}\phi}{\mathrm{d}r}\right) = \frac{n_0 e}{\epsilon_0}\left(\exp\left(-\frac{e\phi}{kT}\right) - \exp\left(\frac{e\phi}{kT}\right)\right) \tag{1.13}$$

[3]Similar behavior can be observed in electrolytes. This case was investigated by Debye and as a result, the effect carries his name.

Anticipating that $e\phi/kT \ll 1$ and using Taylor expansion, 1.13 becomes

$$\frac{1}{r^2}\frac{\mathrm{d}}{\mathrm{d}r}\left(r^2\frac{\mathrm{d}\phi}{\mathrm{d}r}\right) = \frac{2n_0e^2\phi}{\epsilon_0 kT} \tag{1.14}$$

By substituting $\phi' = \phi/r$ and using 1.9 equation 1.14 may be written

$$\frac{\mathrm{d}^2\phi'}{\mathrm{d}r^2} = \frac{2\phi'}{\lambda_D^2}, \tag{1.15}$$

together with the initial condition $\phi = e/(4\pi\epsilon_0)$ as $r \to 0$. Hence the solution of this equation is

$$\phi = \frac{e}{4\pi\epsilon_0 r}\exp\left(-\frac{\sqrt{2}}{\lambda_D}r\right) \tag{1.16}$$

This equation describes Debye shielding. The ion's potential is shielded by the exponential factor, the characteristic length being the Debye length. However, this derivation contains two assumptions. Firstly, the stationary location of the ion and secondly the $e\phi/kT \ll 1$ approximation. The justification of these assumptions can be found in [1].

1.4 Larmor orbits

Consider a charged particle moving in a homogenous magnetic field. Such a particle moves on a circular path. The equation of motion of this particle has the form

$$m\frac{\mathrm{d}\mathbf{v}}{\mathrm{d}t} = e\mathbf{v} \times \mathbf{B} \tag{1.17}$$

If the magnetic field $\mathbf{B}$ is in the direction of the z axis, the components of equation 1.17 can be written

$$m\frac{\mathrm{d}v_x}{\mathrm{d}t} = ev_yB, \qquad m\frac{\mathrm{d}v_y}{\mathrm{d}t} = ev_xB, \tag{1.18}$$

$$m\frac{\mathrm{d}v_z}{\mathrm{d}t} = 0, \tag{1.19}$$

where B is the magnitude of the magnetic field. From 1.19 it is visible that the particle velocity along the magnetic field v_z is constant. By solving the set of equations 1.18 we obtain

$$v_x = v_\perp \sin(\omega_c t), \qquad v_y = v_\perp \cos(\omega_c t), \tag{1.20}$$

where $v_\perp$ is a positive constant meaning the velocity in the plane perpendicular to the magnetic field, and $\omega_c = eB/m$ is the *cyclotron frequency*[4]. By integrating equations 1.20, the coordinates of the particle can be obtained

$$x = -r_L \cos(\omega_c t), \qquad y = r_L \sin(\omega_c t), \tag{1.21}$$

[4] Also termed *gyrofrequency* or *Larmor frequency*.

where r_L denotes the *Larmor radius*

$$r_L = \frac{v_\perp}{\omega_c} = \frac{mv_\perp}{eB}. \tag{1.22}$$

By observing the equations 1.22 and 1.19 it is visible that the particle has a helical trajectory composed of the constant velocity in direction of the magnetic field and circular motion in the plane perpendicular to the field.

Chapter 2

Tokamaks

A tokamak[1] is a device designed to confine plasma in order to achieve thermonuclear fusion. The final goal of these devices is to meet the condition of positive energy balance of fusion. This condition is known as the Lawson criterion[2]. The basic principles of operation of these devices will be described in this chapter.

2.1 Magnetic fields

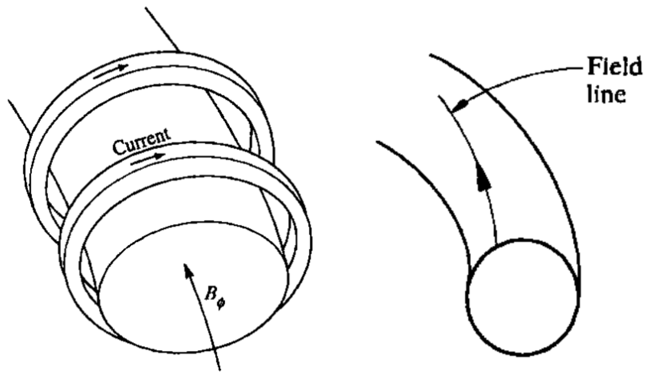

(a) (b)

Figure 2.1: Polodial coils used to generate the toroidal magnetic field B_ϕ (a) and the resulting helical magnetic field of the tokamak (b) [J. Wesson, Tokamaks].

A tokamak is a magnetic confinement system of toroidal shape. Its magnetic field is a superposition of two distinct fields, the principal being a toroidal field, which would however not be able to confine the plasma alone, so an additional poloidal field is present. The toroidal field is produced by external coils shown in Fig. 2.1(a), while the poloidal field is caused by current flowing in the plasma itself in the toroidal direction. The sum of these

[1]The word tokamak is a transliteration of the Russian "toroidal'naya kamera s magnitnymi katushkami" - toroidal chamber with magnetic coils.

[2]Published by John D. Lawson in 1957, the criterion describes a condition for density, confinement time and temperature of a plasma. When satisfied, the fusion reaction in the plasma is self-sustainable. The exact form of the Lawson criterion depends on the specific reaction. The rigorous derivation of the criterion can be found in [1, 2]

fields gives rise to helical magnetic field lines along the torus, shown in Fig. 2.1(b). Each magnetic field line lies on a toroidal *flux surface*, as shown in 2.2(a).

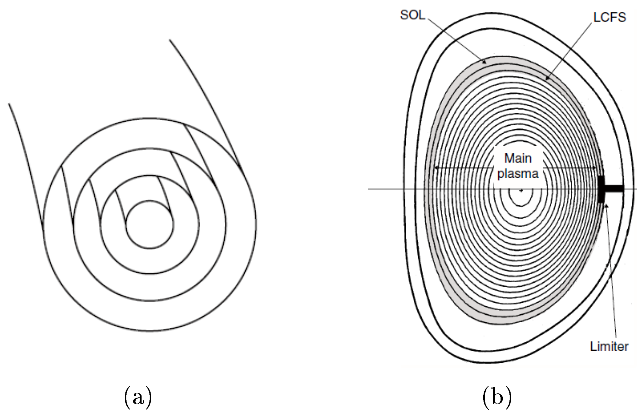

Figure 2.2: Magnetic flux surfaces forming a set of nested toroids (a) and poloidal cross-section of a tokamak with the LCFS and SOL highlighted (b). [P. C. Stangeby, The plasma boundary of magnetic fusion devices].

Tokamak plasmas are bounded by a solid surface, which is called a *limiter*. Magnetic field lines which lie on surfaces that never touch a solid surface are called *closed*. Those which intersect a solid surface, are called *open*. A very important role is played by the *last closed flux surface*, LCFS. Naturally, it is the last flux surface that does not touch a solid surface, Fig. 2.2(b). Surfaces radially further inwards are all closed while surfaces further outwards are all open. The LCFS will play a key role in chapter 3. The region radially outwards the LCFS is termed the *Scrape-off layer*, SOL.

In order to achieve thermonuclear conditions in a tokamak (given by the Lawson criterion) high temperatures and densities are necessary. However, when temperature and density increases, so does plasma pressure. Higher pressure can be confined by a stronger magnetic field, yet the magnitude of the toroidal field is limited by technological factors. With present technology it seems likely that the maximum magnetic field at the coils would be around 12 T [2].

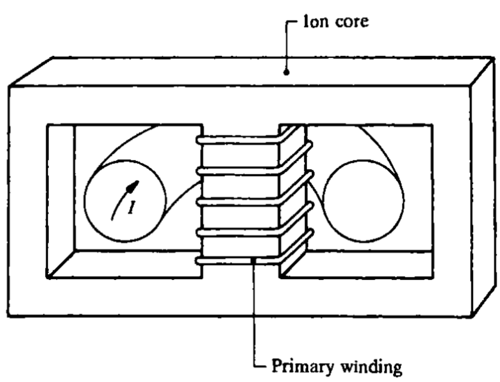

Figure 2.3: Primary winding and iron core used to cause flux change in the torus. [J. Wesson, Tokamaks]

The plasma pressure which can be stably confined increases with toroidal plasma current for any given toroidal magnetic field, but only to a limited value. The poloidal field produced by the toroidal current is usually an order of magnitude smaller than to toroidal field. In present large tokamak experiments, currents of several MA are used. The plasma current is driven by a toroidal electric field that is induced by a transformer. Change of flux is caused by a current passed through a primary coil around the torus as shown in Fig 2.3. An iron transformer core is often used in order to reduce the power supply and to suppress stray magnetic fields.

2.2 Energy confinement

To achieve thermonuclear conditions in a tokamak it is necessary to confine the plasma for a sufficient amount of time. The global energy confinement time τ_e is defined by

$$\tau_E = \frac{W}{P} = \frac{\int \frac{3}{2} nk(T_e + T_i)\mathrm{d}V}{P}, \tag{2.1}$$

where W is the thermal energy of the plasma, P is the total power input, n is the plasma density and T_e and T_i are the electron and ion temperatures respectively. Confinement is limited by thermal conduction and convection, but also by radiation. So far, there is no consistent theory that explains all the processes limiting the confinement of plasma in tokamaks. To be more specific, the transport of particles and energy, which would occur in a toroidal plasma with no instabilities has been calculated. Unfortunately, the transport that really does occur strongly disagrees with the calculated values. The cause of this abnormal transport is thought to be in instabilities, which allow unpredicted transport across the structure of the magnetic field or local break-down of the magnetic field itself. Although many types of fluctuations of various sorts have been predicted and observed in tokamaks, their relation to the resulting transport is not clear.

Provided the need to predict confinement properties, empirical methods are used. Data from many tokamaks, each operated under a range of conditions is collected to extrapolate the behavior of future devices.

One could suggest to use a classical transport model for a cylindrical plasma, as decribed in [2] to calculate the confinement time. This model is unsuitable for a torus[3] though, even if the plasma temperature is low which means the plasma is very collisional. A toroidally induced force is present, leading to an internal convective flow outward along the major radius. This is called Pfirsch-Schlüter transport and the total transport is larger than by using the mere cylindrical model. At higher temperature, the fluid model itself is inapplicable. Particles travel on trajectories determined by the magnetic field due to low collisionality. Particles trapped in the outer side of the torus gyrate in banana orbits, whose width is $(q/\sqrt{\epsilon})r_L$, where r_L is the Larmor radius, q is the safety factor[4] and ϵ is the aspect ratio, $\epsilon = R/r$ where R is the major radius and r is the minor radius of the torus. These larger orbits allow larger steps resulting from collisions than particles gyrating with Larmor orbits.

The energy confinement time taking Pfirsch-Schlüter transport and banana regime transport in account with respect to density, temperature, poloidal magnetic field B_p and plasma size

[3] The collisional transport in a torus is known as neoclassical.

[4] The safety factor characterizes the stability of a plasma and is defined as the number of toroidal circuits of a field line until one poloidal circuit is achieved. For a tokamak with circular cross section, $q \approx \frac{rB_\phi}{RB_\theta}$. It is also an important factor in transport theory [2].

l is approximately

$$\tau_E \sim \frac{(kT)^{\frac{1}{2}} B_p^2}{n} l^2. \tag{2.2}$$

Experimental confinement times are not only much shorter , but unfortunately they even do not follow the scaling given by 2.2. However, as was previously mentioned, empirical scaling can be helpful. A scaling obtained by R. J. Goldston, for auxiliary heated tokamaks, has proved to be adequate over a wide range of parameters. This scaling has the form

$$\tau_E \sim \frac{B_p^2}{nkT} l^{1,8}. \tag{2.3}$$

However, it was discovered, that under certain circumstances there is an abrupt change in confinement as the heating power is increased. The confinement time increases typically by the factor two. This regime is called the *H-mode*[5]. The previous lower level regime is called the *L-mode*. The confinement in the H-mode improves mainly due to the appearance of a transport barrier at the edge of the plasma.

2.3 Heating

The D-T plasma[6] must be heated to thermonuclear conditions described in the previous section. As the plasma is heated, the internal alpha particle heating provides an increasing fraction of the total heating, until a point where plasma temperature can be sustained only by alpha particle heating is reached. The applied external heating can then be removed and the plasma becomes self-sustaining. This event is called ignition. The power balance can be written

$$P_H + P_\alpha = P_L \tag{2.4}$$

Where P_H is the power of external heating, P_α is the power resulting from the alpha particles and P_L is the power loss. For a D-T reaction,

$$P_\alpha = \frac{1}{4}\overline{n^2 \langle \sigma v \rangle} \epsilon_\alpha V \tag{2.5}$$

and

$$P_L = 3\frac{\overline{nkT}}{\tau_E} V, \tag{2.6}$$

where $\langle \sigma v \rangle$ is the reaction rate, n is the density, ϵ_α is the energy of the released alpha particle. By substituing 2.5 and 2.6 into 2.4 we obtain

$$P_H = \left(3\frac{\overline{nkT}}{\tau_E} - \frac{1}{4}\overline{n^2 \langle \sigma v \rangle} \epsilon_\alpha \right) V. \tag{2.7}$$

At ignition, the two terms in the brackets are equal.

[5] The H-mode was discovered on the ASDEX tokamak in 1982.

[6] The deuterium-tritium fusion reaction is by far the most preferable. This is given by the fact that the D-T reaction has the largest cross-section of the candidate reactions except for unpractically high energies. This matter is discussed thoroughly in [2].

2.3.1 Ohmic heating

The initial heating in all tokamaks comes from the ohmic heating caused by the toroidal current. Ohmic heating is powerful mainly in the lower temperature region and can produce temperatures of a few keV. Nevertheless, as the temperature increases, resistivity falls as $T^{-\frac{3}{2}}$ as a consequence of reduced collision times. At temperatures required for ignition, ohmic heating is reduced and other ways of heating must be applied.
There are two main methods used to heat the plasma to ignition temperatures, the injection of energetic neutral beams and the absorption of radio frequency electromagnetic waves. Both of these methods would be capable of providing heating of sufficient magnitude.

2.3.2 Neutral beam injection

Using the first method, high energy neutral atoms are injected into the plasma. Since the atoms are neutral, they travel in straight lines in the magnetic field. However, through collisions, the neutral atoms become ionized and travel in orbits determined by their energy, the present magnetic field, angle of injection and point of deposition. It is important that as much of the deposition as possible should take place in the central region of the plasma to avoid heating of the plasma edge and particle sputtering of the material surfaces. Once the neutral beam particles become ionized, the resulting fast ions are slowed down by Coulomb collisions. The former beam atoms thermalize, while energy is passed to the particles of the plasma.

2.3.3 Radio frequency heating

The second method, radio frequency heating (RF), transfers energy to the plasma from an external source by means of electromagnetic waves. The waves accelerate the plasma particles, thus heating the plasma as a whole. However, just like ohmic heating, at high temperatures collisional absorption of electromagnetic waves is ineffective as a direct heating mechanism for hot plasmas. The mechanism used is called resonant absorption. A magnetized, multi-species plasma has several resonant frequencies which enable absorption of the energy of an incident wave. The general layout consists of a powerful generator outside the plasma, a low loss transmission line and an antenna which supplies the electromagnetic energy to the plasma. Once introduced to the plasma, the electromagnetic waves are required to travel, with negligible loss, to the zone of absorption. The heating scheme is usually designed in a way that the absorption zone is externally controllable. Models of propagation of waves in a plasma and several frequency schemes can be found in [2].

2.4 Tokamak experiments

A variety of tokamak experiments is or was in operation in research laboratories throughout the world. Here, the TCV and JET experiments will be briefly introduced, since in further parts of this thesis simulations using TCV and JET input parameters will be desribed.

2.4.1 TCV

TCV is the acronym for Tokamak à configuration variable and is an experimental device of the École polytechnique fédérale de Lausanne, in Switzerland. It has a major radius of 0.89 m and a minor radius of 0.25 m. The device is able to create and control shaped plasmas,

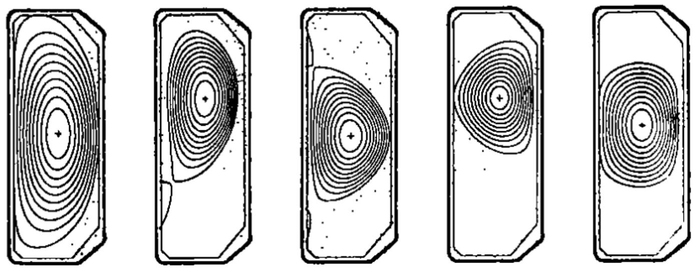

Figure 2.4: Examples of plasma configurations on TCV, demonstrating the shaping capability of the device. [J. Wesson, Tokamaks]

particularly highly elongated plasmas [2], giving the tokamak its name. The vacuum vessel is nearly rectangular, visible in Fig. 2.4 where examples of obtainable plasma shapes in the device are depicted. Experience gained on TCV helps to design the tokamak as a reactor concept.

2.4.2 JET

JET stands for Joint European Torus, since it is a joint undertaking of 16 European states with the support of EURATOM. It is situated in Oxfordshire, UK. Since 2000, the scientific programme has been conducted by the European Fusion Developement Agreement (EFDA). The tokamak has a major radius of 2.96 m and the minor radius was adjusted from the original 1.25 to 1 m. It operates at 3.8 T magnetic fields and plasma currents of up to 7 MA have been reached in limiter experiments. An iron transformer core is installed on the tokamak, improving the efficiency of the primary circuit and reducing stray magnetic fields. The main goals of this experiment is the investigation of the heating and confinement under reactor relevant conditions and also the study of plasma-solid interactions and α-particle production [2]. The size of the tokamak can be appreciated from figure 2.5.

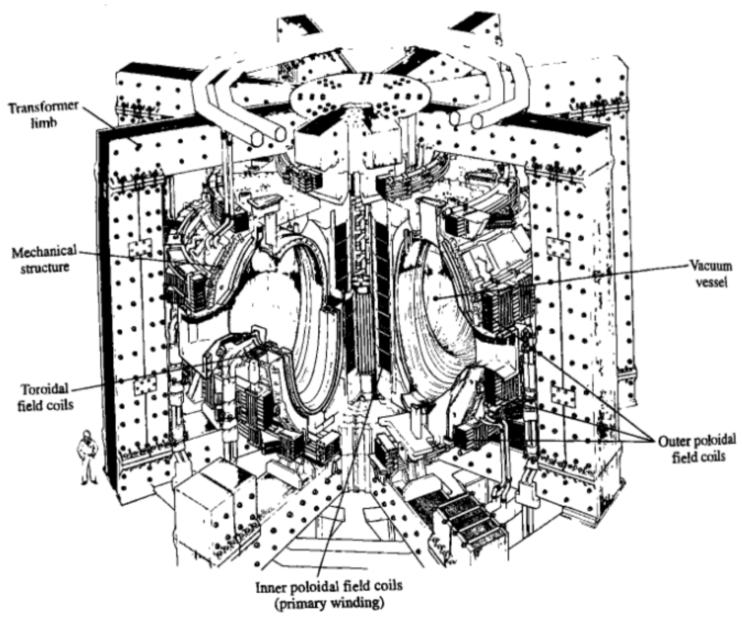

Figure 2.5: Illustrative layout of the JET experiment. [J. Wesson, Tokamaks]

Chapter 3

Edge plasma

Tokamak plasmas always involve interaction with the solid state. This interaction takes place at the plasma edge, where the actual containement vessel begins, and can have significant effects on the plasma as well as the solid surface. This chapter will try to introduce and describe the most important of these effects.

3.1 Scrape-off layer, SOL

In magnetic confinement systems the plasma is confined in closed magnetic flux surfaces. Closed magnetic fields can only be generated within a restricted volume, thus there exists a boundary defined by the last closed flux surface, LCFS, described in section 2.1. The region radially outward from the last closed flux surface is termed the *scrape-off layer, SOL*. The shape of the LCFS is determined by the magnetic fields. Nevertheless, closed magnetic surfaces may be intersected by a solid surface. Such a solid surface is called a *limiter*. Alternatively, the closed surface may be determined completely by the magnetic field so that outside the LCFS, the plasma flows toward and interacts with the solid surface. This system is called a *divertor*. Both systems will be introduced in sections 3.2 and 3.3 respectively.

The SOL can be unfolded and straightened out into an orthogonal block, Fig. 3.1. The block is bounded by opposite solid surfaces. In case of a limiter configuration, these can be two faces of a single poloidal limiter, see section 3.2. In the case of a divertor configuration, the surfaces are defined by opposite divertor plates, section 3.3. The distance between two limiter surfaces or divertor plates (with respect to the field lines) will be denoted $2L$, for reasons that will be clarified later. The top boundary of the block is the actual LCFS and the bottom can be chosen as the vessel wall. The last two sides can be defined in an arbitrary way. For example, the boundary defined by an arbitrary cut can be used, in order to include the whole plasma volume.

Plasma particles which move freely along the magnetic field lines in the SOL have velocities of the order of the plasma sound speed [3], c_s, and so the characteristic *particle dwell time* in the SOL is

$$\tau_{\mathrm{SOL}} \simeq \frac{L}{c_s}. \tag{3.1}$$

For a JET-sized tokamak, $\tau_{\mathrm{SOL}} \approx 1$ ms. It can be seen that dwell times are very short compared to energy confinement times of the main plasma which, for JET, are of the order

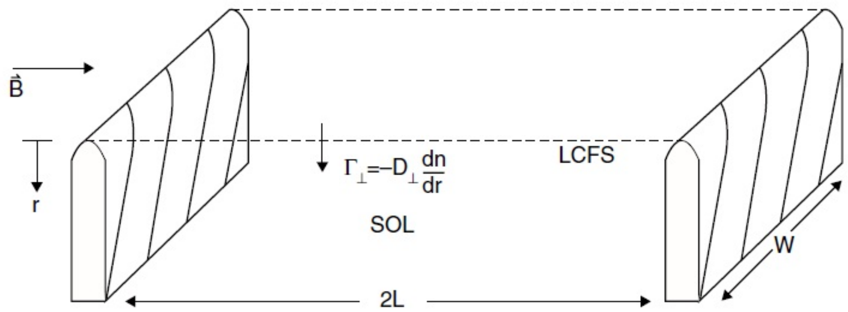

Figure 3.1: The SOL straightened out into an orthogonal block. The bottom and top boundary is the vessel wall and the LCFS respectively, while the other two solidly depicted boundaries are either limiter surfaces or divertor target plates, section 3.3. The remaining two boundaries are arbitrary. [P. C. Stangeby, The plasma boundary of magnetic fusion devices]

of 1 s [3].

3.2 Limiters

As stated in section 3.1., a limiter is a solid surface defining the position of the LCFS. Inserting some kind of limiter into the plasma enables to determine the shape of the confined plasma. The choice of the material of which the limiter is made allows to influence the plasma-solid interaction. Since it has to protect the wall from the plasma when there are disruptions, runaway electrons and other instabilies, it is commonly made of refractory material as carbon, tungsten or molybdenium which are capable to withstand high heat loads. Limiters also localize the plasma-solid interaction.

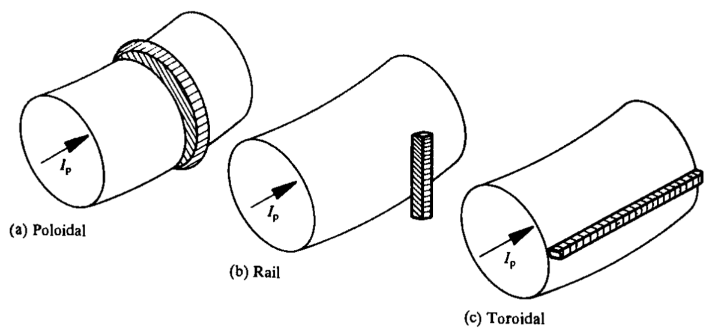

Figure 3.2: Various types of limiters. [J. Wesson, Tokamaks]

The most common limiter geometries are the toroidal, poloidal and rail limiters, Fig. 3.2. The *poloidal limiter* is a metal diaphragm placed usually in one or sometimes in more positions along the torus. It is used in devices whose poloidal cross-section is circular, for example the CASTOR/GOLEM or FTU tokamak [7]. A typical distance a particle travels in the SOL is termed the *connection length* and can approximately be expressed as

$$L \approx \frac{\pi R}{n_{\mathrm{lim}}}, \tag{3.2}$$

where n_{lim} is the number of poloidal limiters along the torus.
A *Toroidal limiter* is a rail covered by protecting plates which is placed into the vacuum vessel all along the toroidal direction. It is usually situated at the bottom of the torus. For example, the Tore Supra and TEXTOR tokamak experiments use this kind of configuration [7]. In this case, the particles need to go around the torus several times before hitting the limiter, thus the connection length L depends also on the safety factor and can be expressed [2] approximately as

$$L \approx \pi R q \tag{3.3}$$

For the rail limiter, depending on its size and the edge value of q, the connection length will still be longer. To give an example, a lithium rail limiter is used on the T-11M tokamak [11].

In principle, any object that is able to close the magnetic field lines on itself can be regarded as a limiter. Another system is the *wall limiter*, where the limiter is the actual vessel wall. The advantage of this system is that the power flux is distributed to a larger surface than in case of the poloidal or toroidal limiter configurations.

3.3 Divertors

In the case of limiters, the LCFS is defined by a solid surface, where impurity atoms are released into the plasma. This is undesirable, since impurities cause radiation losses, exacerbating energy confinement. When using a divertor configuration, the LCFS is defined solely by the magnetic field and plasma-surface interactions occur far away from the confined plasma, which is the main advantage of divertors over limiters. By far the most common type of divertor configuration is the *poloidal divertor*[1], shown schematically in Fig. 3.3. It is formed by a toroidal conductor carrying a current I_d which is parallel to the plasma current I_p and is of the same direction. The two currents generate eight-shaped magnetic flux surface poloidal cross-sections. A point of intersection of the magnetic field lines exists, called the *X-point*, where the poloidal magnetic field is zero. The LCFS which also passes through the X-point is termed the *separatrix*. The region inside the separatrix contains the main or confined plasma and is termed the *confinement region*. In order to localize the plasma-surface interaction, a solid plane is introduced that cuts through flux surfaces surrounding the I_d channel, Fig. 3.3. The solid planes mentioned above are called *divertor target plates* and, as described in section 3.4., the cross-field velocity of the particles in the SOL is small compared to the velocity along the field lines, causing the particles to move rapidly towards the target plates instead of diffusing far away cross-field. Thus, any plasma particle diffusing perpendicularly through the separatrix from the confinement region is eventually swept to the divertor target plates.

Impurity radiation from the divertor targets can dissipate a significant fraction of the power entering the SOL. However, contamination of the confinement region is unacceptable. A way of decreasing the particle flux reaching the target for given upstream conditions is to reach the so-called *divertor detachment*. Hence, detachment is a state at which a drop of particle flux to the divertor target occurs. To achieve detachment, temperatures lower than a few eV and volumetric momentum and power losses are necessary [3].
Furthermore, the strong magnetic shear around the X-point is an important ingredient for

[1]The divertor geometry shown in Fig. 3.3 is termed poloidal because it is the poloidal magnetic field that has been diverted by I_d, although it is toroidally symmetric. This nomenclature can cause confusion.

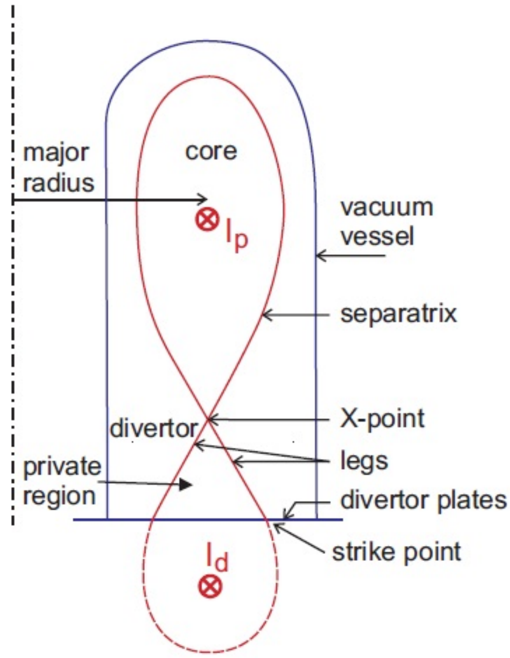

Figure 3.3: The divertor configuration. The poloidal field created by the plasma current I_p is diverted by the field created by the divertor current I_d. [J. Brotánková, Studium horkého plazmatu v experimentálních zařízeních typu tokamak]

achieving improved confinement [7], the H-mode.
The construction of a divertor is obviously more difficult than the construction of a limiter, since it requires an external coil conducting the current I_d which is comparable to the plasma current I_p. Thus this more expensive configuration is used on larger European facilities as JET, COMPASS, ASDEX-U, TCV and MAST and will be used on ITER as well.

3.4 Transport in the SOL

Diffusion across the magnetic field lines is important for plasma confinement. As stated in section 2.2., transport in the confined region is anomalous, making the calculation of the diffusion coefficient impossible. However, the diffusion coefficient in the SOL can be estimated from simple principles.
To roughly estimate the diffusion coefficient in the SOL, $D_\perp^{\mathrm{SOL}}$ the following consideration will be used [7]. In the SOL, the velocity of particles along the magnetic field lines dominates the velocity in the cross-field direction. Particles are penetrating from the confined area, so the source of the particles is the LCFS. At the point that they reach the SOL, they are unable to return to the confined area and they leave in the parallel direction to the limiter or divertor plates. The total particle flow coming from the confined area through the last closed flux surface is

$$\Phi_\perp = -D_\perp^{\mathrm{SOL}} \left.\frac{\mathrm{d}n}{\mathrm{d}r}\right|_{\mathrm{LCFS}} S, \tag{3.4}$$

where $S = 2Lw$ is the surface of the LCFS, Fig. 3.1. Assuming that the density decays radially, a characteristic length of radial density decay λ_n can be defined [3]

$$\lambda_n = -\left(\frac{1}{n}\frac{\mathrm{d}n}{\mathrm{d}r}\right)^{-1}, \tag{3.5}$$

and so the decrease of density can be expressed as

$$\frac{\mathrm{d}n}{\mathrm{d}r} = -\frac{n}{\lambda_n}. \tag{3.6}$$

Equation 3.4 can now be written as

$$\Phi_\perp = -D_\perp^{\mathrm{SOL}}\frac{n_{\mathrm{LCFS}}}{\lambda_n}2Lw. \tag{3.7}$$

The total particle flow to the two solid surfaces in the parallel direction is

$$\Phi_\parallel = 2w\int_{r=\mathrm{LCFS}}^{\infty} nc_s \mathrm{d}r. \tag{3.8}$$

The Bohm-Chodura sheath criterion has been used here [3]. The integral in 3.8 will be approximated by $nc_s\lambda_n$. This can be done if c_s is constant along r and if the density decays exponentially, $n(r) = n_{LCFS}\exp\big(-\frac{r}{\lambda_n}\big)$. This dependence is found to hold approximately by experiment. Hence

$$\Phi_\parallel = wn_{\mathrm{LCFS}}c_s\lambda_n. \tag{3.9}$$

The particle balance states that all the particles coming from the LCFS in the perpendicular direction leave to the limiter or divertor plates in the parallel direction provided the higher velocity in the parallel direction, thus $\Phi_\perp = \Phi_\parallel$ and subsequently the diffusion coefficient is

$$D_\perp^{\mathrm{SOL}} = \frac{c_s\lambda_n^2}{2L} \tag{3.10}$$

$D_\perp^{\mathrm{SOL}}$ can for example be evaluated from Langmuir probe[2] measurements of radial electron density profiles $n_e(r)$. λ_n can be calculated by fitting these profiles, thus determining $D_\perp^{\mathrm{SOL}}$.

The model described above has some limitations, however. According to recent research, transport in the SOL is influenced by turbulence. For example, ELMs[3] in the edge plasma can increase the transport by an order of magnitude. As the turbulence is developed in the inner layers of the plasma, the diffusion coefficient ceases to be a local variable since it can depend on parameters in the confinement area also [7]. The model described above is called the *simple SOL*. A more specific type of SOL, the *two-point divertor SOL* will be described in section 3.7. More complex models of the SOL can be found in [3].

3.5 The divertor SOL

One of the main goals of using a divertor is the achievement of a large temperature drop along the length of the SOL and a temperature of less than 10 eV at the divertor target

[2]Electrical probes used to measure the electron temperature T_e and density n_e, especially at the plasma edge. Their function will be described in section 4.1

[3]ELM stands for *edge-localized mode*, a temporary effect usually characterizing the H-mode, involving periodic expulsions of particles and energy from the main plasma into the SOL [3].

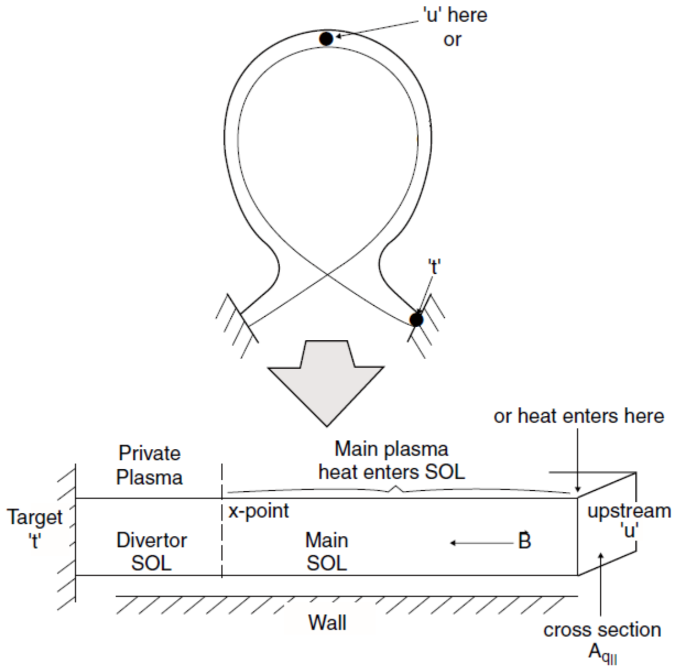

Figure 3.4: The divertor SOL straightened out. [P. C. Stangeby, The plasma boundary of magnetic fusion devices]

[3] in order to achieve plasma detachment as described in section 3.3. In this section, the basic two-point model of the divertor SOL will be described. One of the two points is the "u" location, termed the *stagnation point* in Fig. 3.4 which is taken to be half-way between targets. The model assumes a single X-point divertor geometry. The second point, "t" in Fig. 3.4, is taken to be the actual divertor target.
For modelling purposes, the SOL will be straightened out, as seen in Fig. 3.4. Here, the simplest divertor model[4] will be described, only relating upstream and target conditions, for example the relation between T_{eu} and T_{et}.
Next, the principal assumptions of the two-point model will be desribed.
Firstly, particle balance is assumed. This means that neutrals recycling from the targets are all ionized in a thin layer immediately in front of the target. Furthermore, a neutral which was produced by an ion impacting the target while traveling on a specific magnetic field line is assumed to be re-ionized on the same field line. Thus, the only non-zero parallel plasma flow is in a very thin layer between the ionization point and the target. In this thin layer the flow velocity increases from zero at the start of the ionization zone up to the sheath entrance speed which is taken to be the sound speed. The second assumption is the pressure balance. No friction between the plasma flow in the ionization region and no viscosity effects are assumed. Hence, in the entire length of each flux tube

$$p + nmv^2 = const, \tag{3.11}$$

where p is the static plasma pressure. The electron and ion temperatures are assumed

[4]The described simple divertor model is sometimes called the zero-dimensional, 0D model.

to be the same, $T_e = T_i$, so the static plasma pressure

$$p = nkT_e + nkT_i = 2nkT. \tag{3.12}$$

For the entire length of the flux tube from "u" to the start of the thin ionization layer $v = 0$. At the target, $v_t = c_{st} = \frac{2kT_t}{m_i}^{1/2}$. Then the relation between the upstream and target total pressures is obviously

$$2n_tT_t = n_uT_u. \tag{3.13}$$

The third assumption deals with power balance. Parallel heat convection is absent since $v = 0$ over almost all of the flux tube length. Thus the parallel flux density is all carried by conduction. If the parallel heat convection density $q_{\|}$ entered entirely at the upstream end and was removed at the target at a distance L downstream, then according to [3] the temperatures at the two points satisfy the equation

$$T_u^{7/2} = T_t^{7/2} + \frac{7}{2}q_{\|}\frac{L}{\kappa_{0e}}, \tag{3.14}$$

where κ_{0e} is the electron parallel conductivity coefficient, while parallel ion heat conductivity is neglected. There exists a temperature change across the ionization zone but as it is very thin, T_t in 3.13 is taken to be the target sheath edge temperature. Following [3], for $q_{\|}$ the following equation holds

$$q_{\|} = q_t = \gamma n_t kT_t c_s, \tag{3.15}$$

where q_t is the heat flux density entering the sheath and γ is the sheath transmission coefficient.
Equations 3.13, 3.14, 3.15 are three equations for three unknowns, n_t, T_t, T_u while n_u and $q_{\|}$ are regarded as control parameters and L, γ and κ_{0e} are constants. These equations sum up the two-point model of the divertor SOL. We treat n_u and $q_{\|}$ as control parameters since tokamak operators can regulate the input power and the main plasma density. So far, radial variation of n_u, T_u, n_t, T_t have been ignored. In a more refined approach, we can split the SOL to a range of individual flux tubes and apply equations 3.13, 3.14, 3.15 to each of them. The SOL is now radially divided into long, narrow constant cross-sectional regions aligned with B along which particles travel to the target plates.
As stated earlier, this divertor model is the most simple one. Additional refinements and corrections to this model, as well as more complex models can be found in [3].

3.6 The plasma sheath

In this section, the electric field arising in a very thin layer near a material surface, the *plasma sheath*, will be described. This field will play an important role in chapter 5.
The electron thermal velocity is larger than that of the ions by the square root of the mass ratio. However, in a narrow sheath near the surface, an electric field is set up which decreases the flow of electrons and increases the ion flow, leveling the two flows out. The width of this narrow sheath is several Debye lengths. The differential equation for the potential V, derived thoroughly in [2], has the form

$$\frac{\mathrm{d}^2V}{\mathrm{d}x^2} = \frac{n_0e}{\epsilon_0}\left(\exp\frac{eV}{kT_e} - \left(\frac{\frac{1}{2}m_iv_0^2}{\frac{1}{2}m_iv_0^2 - eV}\right)^{1/2}\right) \tag{3.16}$$

where n_0 is the plasma density, v_0 is the velocity at which ions enter the sheath. The potential at the sheath edge is defined to be zero and it is assumed that the electrons have a Boltzmann distribution. The value of v_0 is determined by requirig that the solution of 3.16 in the narrow sheath edge matches the slowly varying small plasma potential outside the sheath. Hence, by taking a small ϕ, using series expansion and 1.9, equation 3.16 can be written

$$\frac{\mathrm{d}^2 V}{\mathrm{d}x^2} = \left(1 - \frac{T_e}{m_i v_0^2}\right) \frac{V}{\lambda_D^2} \tag{3.17}$$

A slowly varying solution of 3.17 requires

$$v_0 \simeq \sqrt{\frac{T_e}{m_i}} \tag{3.18}$$

The performed calculation has neglected the ion temperature. So, equation 3.18 can be generalized as $v_0 = c_s$, where $c_s^2 \simeq (T_e + T_i)/m_i$. Hence, the plasma enters the sheath at the sound speed.
However, the actual form of the potential across the sheath is not determined from equation 3.17. According to [2] it is derived by the requirement that the total current to the surface be zero[5]. Including the effect of secondary electrons produced at the surface by electron and ion bombardment, the form of the potential is

$$V_{fl} = -\frac{1}{2} \frac{T_e}{e} \ln \left(\frac{(1-\delta)^2 \frac{m_i}{m_e}}{2\pi (1 + \frac{T_i}{T_e})} \right), \tag{3.19}$$

where δ is the total secondary electron emission coefficient due to ions and electrons. This potential is termed the floating potential and is denoted V_{fl}
The energy of the ions that reach the solid surface is determined by the initial thermal energy at which they reach the sheath and the sheath potential V_{fl}, given by equation 3.19, through which they fall. Ions are accelarated in the sheath and their distribution at the surface is approximately an accelerated and truncated Maxwellian. Electrons, however, are decelerated by the sheath, their distribution remaining Maxwellian, but their density is reduced. This happens due to the fact that the sheath potential allows only the high energy tail of the electrons to arrive at the surface. This effect is very important in edge plasma diagnostics, especially for Langmuir probes. The operation of these probes will be described in section 4.1.

3.7 Recycling

When a particle strikes a solid surface, it tends to stick to it for a time long enough to recombine [3]. Ions have a finite probability of back-scattering from the surface. However, they pick up electrons from the surface and re-enter the plasma as neutral particles. Hence, the solid surface acts as a *sink* for a plasma. However, it is not necessarily a mass sink, as the particles are released as neutrals.
Opposite charges are formed on surfaces that are electrically isolated, which leads to surface recombination. The incipient neutrals are not bound to the surfaces and are re-emitted back into the plasma. Consequently, they are re-ionized there. If the plasma charged pairs

[5] This is called the ambipolar condition.

recombine at the surface at the same rate as the emitted neutrals ionize, a steady state is reached. This steady state is termed *recycling*. It is clear that a source of energy is needed to supply the ionization power.

Provided the enormous differences in the properties of the solid state and plasma, the behavior of a plasma can be controlled by the contact it has with a solid surface. The powerful sink activity occuring from the plasma-solid surface interaction is the dominating factor of tokamak edge plasma behavior.

Chapter 4

Edge diagnostics

In this chapter an overview of basic edge diagnostic methods will be given. Measurements by electrical probes, namely Langmuir probes, have been by far the most widely used technique to determine edge plasma parameters [4, 12]. They are also the dominant method to measure low temperature plasmas [13].

4.1 Langmuir probes

Langmuir probes are inexpensive and relatively simple devices. They can be inserted into limiters or divertor targets in large arrays or into reciprocating drive mechanisms for probing deeper in the SOL [14]. In the first case, the probes are non-disturbing for the edge plasma. However, their interpretation is difficult and only a basic theory of operation will be given in this chapter.
The probe is virtually an electrically insulated conductive wire built into the limiter or divertor target plate. The results of section 3.6 induce directly the principles of the operation of a Langmuir probe. An electrically insulated metal object inserted into the plasma (thus electrically "floating") sits at floating potential V_{fl}, see 3.6, relative to the plasma sheath edge, where $V = 0$. Neglecting secondary electron emission, the floating potential has the form

$$V_{fl} = \frac{1}{2}\frac{kT_e}{e}\ln\left(2\pi\frac{m_e}{m_i}\left(1+\frac{T_i}{T_e}\right)\right) \tag{4.1}$$

In this case, the electron and ion flux densities are equal at the probe surface, $\Gamma_i = \Gamma_e$. Next, a probe that is not floating, but that is closed with the plasma via an external circuit will be considered. A potential difference can be applied via an external power supply, see Fig. 4.1. In this case, net current is drawn through the circuit, hence at the probe surface, $\Gamma_i \neq \Gamma_e$. The return surface is the divertor target surface or limiter surface.

By using charge conservation, the net current density to the Langmuir probe can be derived. A rigorous derivation can be found in [3]. The net current density j_{prb} to a probe biased to a potential V has the form

$$j_{prb} = en_{se}c_s\left(1-\exp\left(\frac{e(V-V_{fl})}{kT_e}\right)\right), \tag{4.2}$$

where n_{se} is the electron density at the sheath edge, c_s is the plasma sound speed and T_e the electron temperature at the probe.

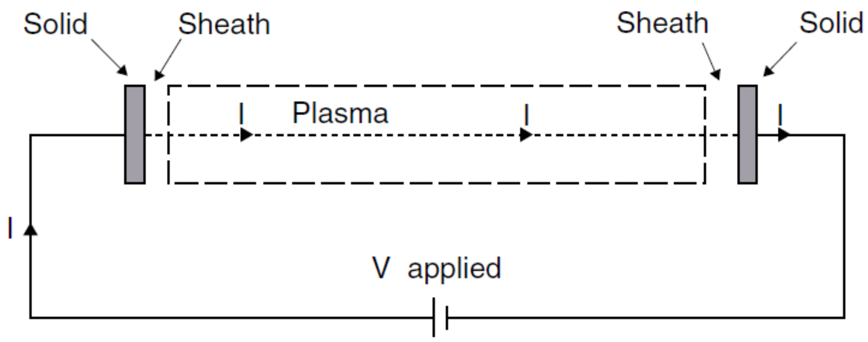

Figure 4.1: The probe circuit with an external power supply. One of the solid surfaces can be considered the probe surface and the other is the return surface. There is either no magnetic field, or **B** lies along the current direction [P. C. Stangeby, The plasma boundary of magnetic fusion devices]

When the probe is biased sufficiently negatively, all the electrons are repelled and all that remains is the ion current. This current is called the *ion saturation current* and is given by the equation

$$j_{sat}^{+} = en_{se}c_s. \tag{4.3}$$

Next, it will be shown that the analysis of the Langmuir probe circuit IV characteristic can yield measurements of the electron temperature T_e and density n_e at the probe. Let A_{prb} be the area of the probe and let the magnetic field $\mathbf{B}$ be parallel to the normal vector of the probe surface. Then the total current passing through the probe is

$$I_{prb} = j_{prb}A_{prb}. \tag{4.4}$$

Combining equations 4.2, 4.3 and 4.4 gives the theoretical IV characteristic of the probe

$$V_{prb} = \frac{kT_e}{e}\ln\left(1 - \frac{I_{prb}}{I_{sat}^{+}}\right). \tag{4.5}$$

Consequently, a logarithmic fit of V_{prb} against I_{prb} yields a measurement of T_e. Since

$$I_{sat}^{+} = A_{prb}en_{se}c_s, \tag{4.6}$$

it can be seen that the fit also yields the electron density at the sheath edge, very close to the probe.

Equation 4.2 holds only for probe potential which are lower than the plasma potential. If the probe potential equals the plasma potential, no sheath electric field is present and electrons are not repelled by the sheath anymore, flowing to the probe at a thermal velocity distribution. This is called electron saturation, and the *electron saturation current* is given by

$$I_{sat}^{-} = -\frac{1}{4}ne\langle v_e\rangle, \tag{4.7}$$

where $\langle v_e\rangle$ is the electron thermal speed and n is the electron density just at the probe. Since electrons carry the same absolute charge but are much lighter, electron saturation current is greater than the ion saturation current by the ratio $(m_i/m_e)^{1/2} \approx 60$ for a hydrogen plasma. However, for values of V_{prb} causing electron saturation, currents drawn from the plasma are so large and disturbing that any simple analysis trying to solve the problem fails. The effect of electron saturation on Langmuir probe T_e measurements will be discussed in section 4.1.4.

4.1.1 Single probes

The probe described in section 4.1 is in fact the actual single Langmuir probe. The current drawn by the probe from the plasma is returned by either the limiter surface or divertor target plate. The main requirement for a return surface area is that it should be large enough so that a small potential change across the return surface sheath will enable the return current to flow. Hence, the surface carrying the return current must not reach the ion saturation limit before the probe reaches electron saturation. In a hydrogen plasma, the return surface should be larger than the probe area by the electron to ion saturation current ratio, which is typically ≈ 60, section 4.1.

4.1.2 Double probes

A double Langmuir probe is a pair of probe tips close enough to each other so that they are assumed to be exposed to the same plasma conditions. The probes are kept isolated from the torus and are connected across a variable biasing voltage source. Let the currents in each probe tip be I_1, I_2. Taking two identical probes with surface A, defining the power supply voltage $V = V_1 - V_2$, where V_1, V_2 are the respective probe voltages and defining the currents with equation 4.2 the following theoretical relation can be calculated

$$I_1 = I_{sat}^{+} \tanh \frac{V}{2T_e} \tag{4.8}$$

The main advantage of this configuration is that limits the electron current, thus preventing destruction of the probe.

4.1.3 Triple probes

Triple Langmuir probes consist of three tips exposed to the same plasma parameters. One of the probe tips measures the floating potential while the other two are coupled and biased with a constant potential so that one tip draws the ion saturation current and the other an electron current, see Fig. 4.2. The potential V_2 on the electron current drawing tip adjusts itself so that the two currents are of the same size. Let the tips be identical, of surface A. Again, using equation 4.2 and $I_1 + I_2 = 0$,

$$(1 - \exp\left(\frac{e(V_1 - V_{fl})}{kT_e}\right))A + (1 - \exp\left(\frac{e(V_2 - V_{fl})}{kT_e}\right))A = 0 \tag{4.9}$$

Assuming the supply voltage to be large, $kT_e \ll e|V_1 - V_{fl}|$, equation 4.9 gives the following expression for the temperature

$$T_e = \frac{(V_2 - V_f)}{k \ln 2} \tag{4.10}$$

Since in this case V_2, V_{fl} and I_{sat}^{+} can be measured at the same time, high time resolution is an advantage of this arrangement. Thanks to this triple probes are frequently used

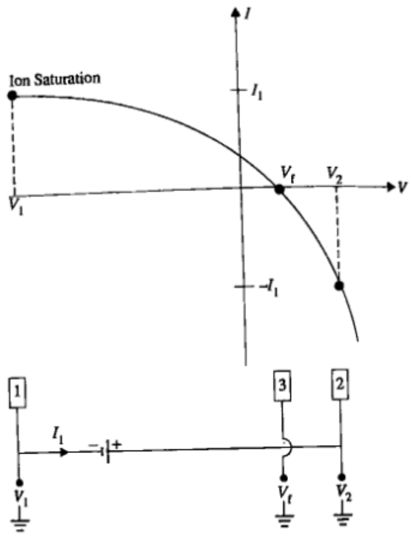

Figure 4.2: Schematic illustration of the triple Langmuir probe configuration. The circuit diagram shows the positions of the probes on the $I(V)$ curve [J. Wesson, Tokamaks]

to measure ELM discharges. Fig. 4.3 shows high time resolution divertor triple probe measurments from JET. However, triple probe data are unreliable in situations when plasma parameters differ across the three probe tips or when I^+_{sat} and I^-_{sat} are comparable [2].

4.1.4 Langmuir probe disadvantages

The main disadvantage of Langmuir probes is that in order to measure spatial temperature or density profiles, they have to be inserted into the plasma, thus there can be a distortion of measurement due to the intrusion of the probe. So, the probe body should be small enough to minimize perturbation.

Another disadvantage is the interpretation of Langmuir probe measurements, which can be quite a challenge, as reported in section 4.1. For non magnetized ($\mathbf{B} = \mathbf{0}$) plasmas it is found, in accord with section 4.1, that the electron to ion saturation current ratio is

$$\frac{j^-_{sat}}{j^+_{sat}} = \left(\frac{m_i}{m_e}\right)^{1/2}. \tag{4.11}$$

However, when $\mathbf{B} \neq \mathbf{0}$ far smaller ratios are usually recorded. It appears that equation 4.1 does not hold for voltages higher than the floating potential, see Fig. 4.4, an experimental IV characteristic from the T-10 tokamak. The data is fitted up to the point where the roll over into electron saturation occurs.The reason for this is not clear. It appears that resistances within the plasma itself have something to do with this problem [3]. So, commonly only the net-ion collecting path is used to obtain measurements of plasma parameters [14]. Unfortunately, this causes that only the tail of the electron distribution, comprising around 5% of the total is measured [2]. If the distribution is non-maxwellian, this can result into incorrect, more precisely too high values of T_e [3] being measured by the standard analysis of the probe IV characteristic. Identifying the causes of the non-maxwellity of the electron distribution and its treatment to achieve a correction to Langmuir probe T_e measurements are the main objectives of chapter 5.

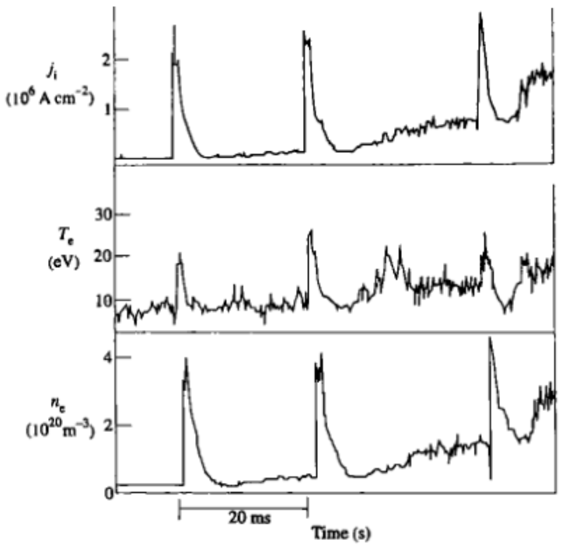

Figure 4.3: Divertor target triple probe measurements during an ELM discharge at JET [J. Wesson, Tokamaks]

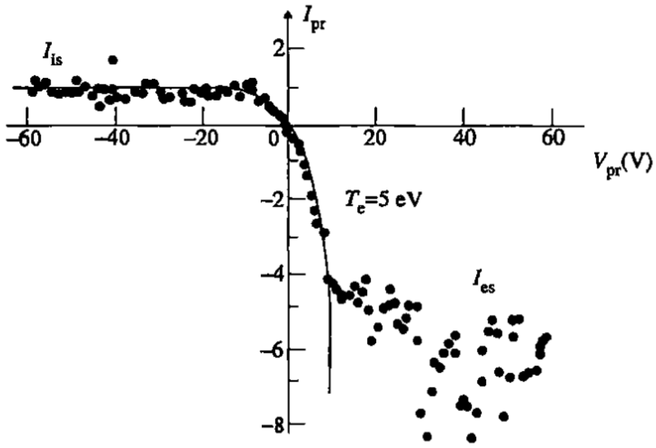

Figure 4.4: A single Langmuir probe characteristic from the T-10 tokamak [J. Wesson, Tokamaks]

Some comparisons with other measurement techniques are shown in Fig. 4.5 and Fig. 4.6. In both figures, it is clearly seen that Langmuir probe measurements yield higher electron temperatures than alternative methods, i. e. lithium beam injection[1] and Thomson scattering.

[1]A diagnostic method involving the Zeeman effect on a high-energy neutral lithium beam injected into the plasma. Both the electron density and temperature can be measured. A detailed analysis on neutral atom diagnostics can be found in [4].

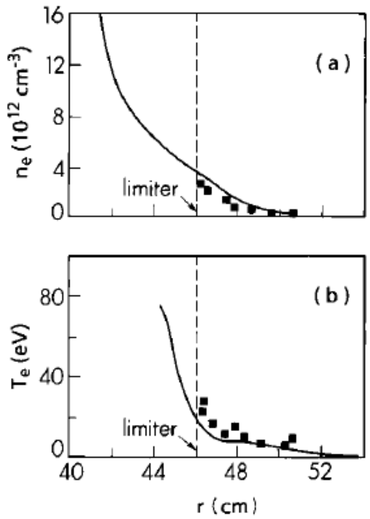

Figure 4.5: Measurements of n_e and T_e in the TEXTOR tokamak using a lithium beam (continuous line) and a Langmuir probe (points). [P. C. Stangeby, G. M. McCracken, Nuclear Fusion, Vol. 30, No. (1990) 1225]

4.2 Other diagnostic methods

Since diagnostics is a very broad topic, only an overview of the other main edge diagnostic methods will be given.

4.2.1 Thomson scattering

Another powerful method to measure plasma temperature and density is Thomson scattering. It is the scattering of laser light by electrons in a plasma. The electron temperature is obtained from the degree of broadening of the spectrum of laser light. For short wavelengths of the incident laser radiation, the scattered spectrum is dominated by a peak of width of order kv_{T_e} so T_e can be determined. The electron density n_e is determined from the absolute level of scattered power. A detailed analysis of Thomson scattering diagnostic principles can be found in [4].

As a contrast to Langmuir probes, Thomson scattering is a non-perturbing method, only requiring acces of radiation to the plasma and can be used to measure parameters in virtually any part of the plasma. It provides the possibility to determine detailed information about the distribution function of electrons and sometimes even ions too [4]. The disadvantage is the great technical diffuculty of the measurents.

4.2.2 Bolometry

Estimating the energy loss from a plasma by radiation is essential for fusion research. Although radiation losses in the plasma center are small, there is significant radiation from the cooler outer regions of the plasma [4]. A direct method to measure the radiative loss is to use a bolometer. A bolometer measures the power of incident radiation via the heating of a material with a temperature-dependent electrical resistance. These devices consist of an absorbing element which absorbes all the incident energy. Thus the temperature of the

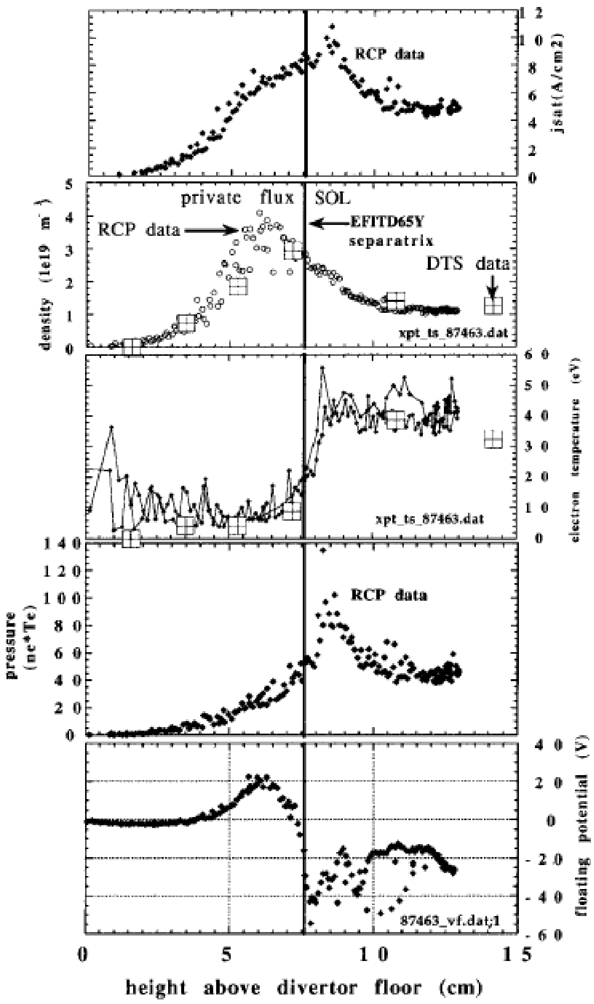

Figure 4.6: Vertical profiles of n_e and T_e above the divertor target floor in the DIII-D tokamak using Langmuir probes (RCP) and Thomson scattering (DTS). [J. G. Watkins, R. A. Moyer, J. W. Cubbertson et al., Journal of Nuclear Materials 241-243 (1997) 645]

element rises and, as the temperature-resistance dependance is known, it can be determined from an IV characteristic. The temperature rise divided by the bolometers thermal capacity is then equal to the total energy flux from the plasma. In most cases an imaging system of bolometers is used so that a spatial reconstruction of the emission profile is possible, rather than a single bolometer at the plasma edge. This allows one to identify where most of the radiation is coming from.

4.2.3 Infrared thermography

This non-perturbative method has become important in edge plasma physics over the last 15 years [20]. In contrast to Langmuir probes, Thomson scattering and bolometry, IR cameras do not measure the temperature of the plasma but they measure the divertor or limiter temperatures instead. This is not surprising since the method is based on black body radiation. All bodies emit thermal radiation which is a function of the temperature and surface properties of the body. The wavelength of maximum radiation intensity is given by Wien's displacement law

$$\lambda_{\text{max}} = \frac{b}{T}, \tag{4.12}$$

where b is Wien's displacement constant and T is the temperature of the body. Broadly speaking, IR detectors measure the spectrum of radiation from the divertor or limiter. The temperature is then determined from Wien's law by finding the peak of the spectrum.

Chapter 5

Analysis of Langmuir probe T_e measurements

As stated in section 4.1, the enhancement of the tail of the distribution function can lead to overestimation of Langmuir probe electron temperature measurements. In this chapter, the possible causes of the non-maxwellity of the distribution function will be described. A simple kinetic model predicting Langmuir probe measurements of T_e at the divertor target will be introduced.

5.1 Background

Langmuir probes are commonly used to measure plasma parameters, such as the electron temperature or plasma density in the plasma edge. It is an inexpensive and relatively simple method, however there is a variety of observations showing that under some specific conditions the electron temperature T_e measured by probes can significantly differ from the actual T_e in the SOL. For example, in [16] it is reported that during ohmic heating in the ASDEX tokamak the T_e measured by Langmuir probes is at least two times higher than the one measured by Thomson scattering. In [5] it is reported that in strongly recombining detached or partially detached divertor plasmas on TCV the expected $T_e \sim 1$ eV is not reproduced by probes. Instead, measured values of approximately $T_e \sim 5$ eV are typical.

Thus from section 4.1 this indicates that the electron velocity distribution function (EVDF) at the plasma edge deviates strongly from a Maxwellian distribution. A reason for this deviation can be fast electrons originating in further upstream of the divertor which may travel collisionlessly to the targets [5]. De-Maxwellization of the EVDF is also affected by a number of processes in the SOL like inelastic collisions of electrons with neutrals and impurities or fast-time processes like edge-localized modes (ELMs) and blobs [8]. In the next two sections, two possible approaches to treat this problem are introduced. The description and interpretation of the latter is one of the main aims of this thesis.

5.2 PIC simulations

In paper [8] a self-consistent, massively parallel PIC[1] simulation is used to calculate non-maxwellian EVDFs at divertor target triple probes at JET. The simulation is performed for

[1] The Particle-in-Cell (PIC) method refers to a technique used to solve a certain class of partial differential equations. In this method, individual particles (or fluid elements) are tracked in continuous phase space,

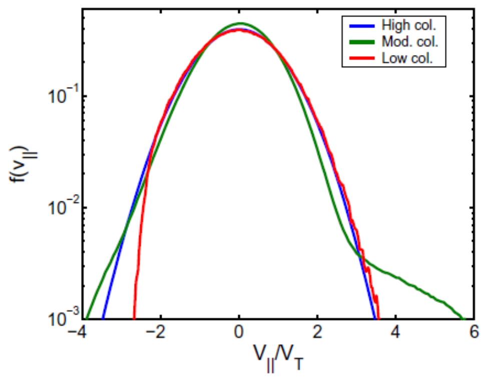

Figure 5.1: Normalized EVDFs at the position of a triple Langmuir probe for stationary SOL with different collisionalities. [D. Tskhakaya et al., Journal of Nuclear Materials 415 (2011) 860-864].

stationary SOL conditions as well as for ELMs. The key player of the simulation is the ratio of elastic and inelastic collisions. In Fig. 5.1 calculated distribution functions for different collisionalities and SOL regimes are shown. Electron collisionality ν^* is defined as the ratio of electron-electron collision frequency and the electron bounce frequency. The bounce frequency is that at which electrons trapped on banana orbits oscillate. The paper concludes that for moderate divertor plasma collisionalities, triple Langmuir probes can overestimate the electron temperature by factor of five. On the contrary, for ELM discharges, probes underestimate peak values of T_e up to 70% [8].

5.3 Simple kinetic model

Self-consistent simulations described in section 5.2 require powerful supercomputers[2] and significant amounts of time to perform the computation. Another approach to the problem is to try to identify and handle the main phenomenon responsible for the non-maxwellity of the EVDF, thus requiring much lower computational power. One of the aims of this thesis is the detailed description and interpretation of the results of such a model, namely the model described in the paper of J. Horáček et al. [5]. The phenomenon behind the de-maxwellization of the EVDF is believed to be the presence of large parallel temperature gradients in the SOL. The parallel T_e gradients lead to the enhancement of the tail of the EVDF and, from section 4.1, probes evaluate the temperature primarily from the tail of the EVDF, hence leading to T_e overestimation. The simulations are carried out for TCV and JET input data.

The idea of the model is the numerical construction of EVDFs at the divertor target, where the electron temperature T_e is measured by Langmuir probes. From the EVDF, Langmuir probe IV characteristics, section 4.1, can be derived.

5.3.1 Input data

whereas moments of the distribution such as densities and currents are computed simultaneously.

[2]All simulations from the paper of D. Tskhakaya et al. [8] have been performed on HECTOR (Edinburgh, UK) and HPC-FF (Jülich, Germany) supercomputers. Times required for a single simulation on 512 processors ranged from 24 to 36 hours.

As an input, the model requires parallel $T_e(x)$ and $n_e(x)$ SOL profiles, where x is the connection distance, starting from position $x = 0$, the inner divertor target plate and ending at $x = L$, the outer divertor target plate. The model also includes potential variation. The potential profile $\phi(x)$ can readily be calculated from the temperature profile, according to [9], as $\phi(x) = 0.71k(T(x) - T(0))$ As stated in section 5.3, the simulation is carried out for TCV and JET input data.

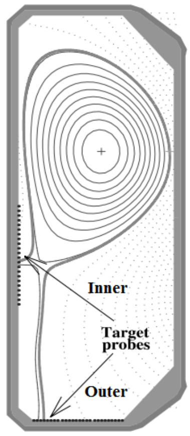

Figure 5.2: TCV equilibrium. The profiles from the highlighted flux surface are used in the kinetic model. [Horacek et al., Journ. nucl. mat., 313-316 (2003) 931-935]

TCV

Experimental data of parallel $T_e(x)$ and $n_e(x)$ are unavailable, thus profiles obtained from fluid simulations were used, in particular, profiles generated by the B2-EIRENE[3] code. The parallel electron temperature and density are the results of any converged solution. The simulation uses results computed by the SOLPS4 B2-EIRENE package with no drifts included and with carbon as the only impurity species [5]. In Fig. 5.3, the parallel T_e and n_e profiles are plotted against the x-coordinate, i.e. the position along the magnetic field line. The profiles are situated in the flux surface at distance 1.8 mm outside the midplane separatrix, which is highlighted in Fig. 5.2. Low density cases may be regarded as low recycling solutions, while higher density corresponds to high recycling conditions [5].

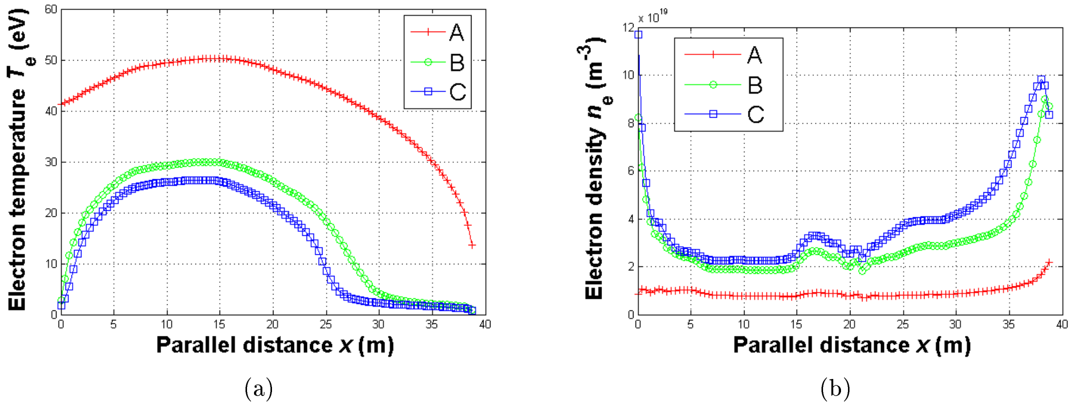

Figure 5.3: Computed parallel T_e (a) and n_e (b) profiles from the B2-EIRENE code, for the flux surface situated 1.8 mm from the separatrix. The labels A, B, C denote increasing midplane density, n_e^m = 8, 23 and 33 .10^{-18} m^{-3} respectively. The x-coordinate spans from the inner divertor target to the outer divertor target.

[3]B2-EIRENE is a two-dimensional plasma edge fluid code. The code package was developed for TEXTOR applications in the late 1980s. It has become a standard tool in plasma edge science. Currently it is mainly used for divertor configurations, also by the ITER central team in order to assist in designing the ITER divertor, see [19]

JET

As experimental data are not available, parallel profiles computed by the EDGE-2D fluid code package are used. Three different profiles E, F, G are visible in Fig. 5.4.

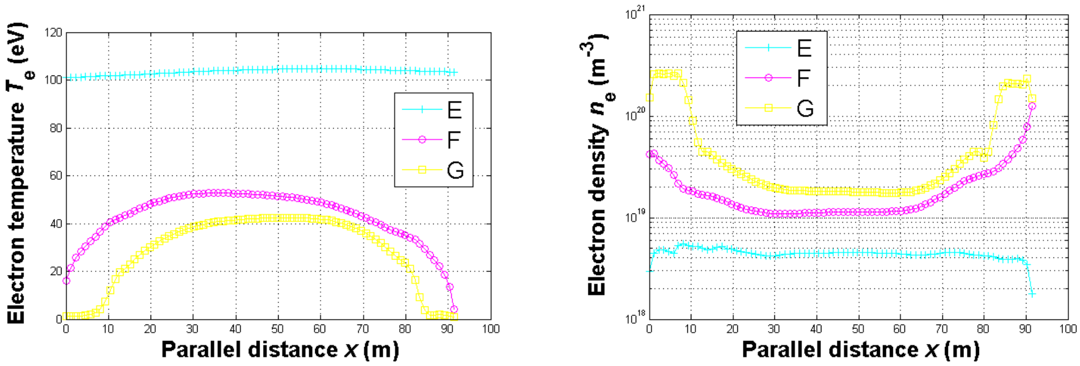

(a) (b)

Figure 5.4: Computed parallel T_e (a) and n_e (b) profiles for the JET tokamak. The labels E, F, G denote increasing midplane density. The x-coordinate spans from the inner divertor target to the outer divertor target. For better visibility, the n_e profile is plotted logarithmically.

5.3.2 EVDF construction

Fast electrons from the warmer upstream regions can travel collisionlessly to the targets, thus affecting the distribution function. The contribution of these electrons to the target EVDF is constructed numerically. The $T(x), n(x), \phi(x)$ profiles are specified, section 5.3.1. The principle of the model:

1. First, a specific value of v_0 is chosen at the target. The x-coordinate at the target is, naturally, $x = 0$.

2. Next, the mean free path $\lambda(0)$ of the electron with velocity v_0 in the target plasma characterised by $T_e(0)$ and $n_e(0)$ is calculated. The choice of the formula for the mean free path will be discussed in section 5.3.4.

3. Now, a smal (constant) step $\mathrm{d}x$ upstream is taken. The x-coordinate of the electron is now $x = 0 + \mathrm{d}x$.

4. Subsequently, the probabilty of a collision occuring during this step is calculated classicaly, $\mathrm{d}p = \frac{\mathrm{d}x}{\lambda}$.

5. During the step, in consequence of the potential change, the velocity changes too. The new velocity is found, from energy conservation: $v(x) = \sqrt{v_0^2 + \frac{2e}{m_e}(\phi(x) - \phi(0))}$.

6. Again, the mean free path $\lambda(v, x)$ is calculated for $T_e(x), n_e(x)$, v and the probabilty of collision during the next step $\mathrm{d}p(x)$ is computed.

7. The procedure described above is repeated. As the electron advances further upstream, the total probablity of collision accumulates. The accumulated probability of collision

at point x_u upstream is the sum of the probabilities of collision during each step and can be written as

$$p(x_u, v_0) = \int_0^{x_u} \mathrm{d}p(x) = \int_0^{x_u} \frac{\mathrm{d}x}{\lambda(v_0, x)} = \int_0^{x_u} \frac{\mathrm{d}x}{\lambda(v(\phi(x), v_0), T_e(x), n_e(x))}. \tag{5.1}$$

8. Naturally, the process is repeated until a point with coordinate x^* is reached, where the accumulated probability of collision reaches unity, i. e. where $p(x^*, v_0) = 1$.

9. It is assumed that a Maxwellian EVDF exists $f^{\mathrm{Max}}(v)$ at every point x along the field line. Since an electron with "terminal" velocity v_0 at the target could have traveled collisionlessly from points $x < x^*$, the target electron velocity distribution function can then be evaluated as the "average" EVDF along to field line from $x = 0$ until the point $x = x^*$ [9]:

$$f(v_0) = \frac{1}{x^*} \int_0^{x^*} S(x) f^{\mathrm{Max}}(T_e(x), n_e(x), v(x, v_0)) \mathrm{d}x, \tag{5.2}$$

   where the weighting function $S(x) = \exp(-p(x))$ represents a suitable electron source distribution [5]. The physical meaning of this weighting function is that electrons originating closer to the target have a greater chance of reaching the target than from sources further upstream, thus EVDFs closer to the target count more in integral 5.2.

10. By repeating this process for a range of values of v_0, the entire EVDF at the target is constructed.

5.3.3 IV characteristic construction

Now that the synthetic EVDF simulating the "real" EVDF at the target is known, the divertor target probe IV characteristic can be constructed. This is done by calculating the *cutoff velocity* v_{cutoff}, the minimum velocity at which electrons can overcome the sheath potential of an electrically floating probe, section 3.6 and 4.1. At the probe(again under floating conditions), the ambipolar condition must be satisfied, i.e. the electron and ion currents must be equal,

$$j_{prb}^- = j_{prb}^+. \tag{5.3}$$

The ions enter the sheath at the sound speed, hence

$$j_{prb}^+ = e n_{se} c_s, \tag{5.4}$$

where n_{se} is the density at the sheath edge and c_s the ion sound speed. The ion and electron temperatures and densities are assumed to be equal, $T_i = T_e, n_i = n_e$, therefore $n_{se} = n_e(0)$ and $c_s = \sqrt{\frac{2kT_e(0)}{m_i}}$. Since the EVDF at the target is known, the electron current to the probe can readily be calculated as

$$j_{prb}^- = e \int_{v_{\mathrm{cutoff}}}^{\infty} v_0 f(v_0) \mathrm{d}v_0. \tag{5.5}$$

Thus by substituting 5.4 and 5.5 into the ambipolar condition 5.3 the following equation is obtained

$$\int_{v_{\text{cutoff}}}^{\infty} v_0 f(v_0) \mathrm{d}v_0 = \sqrt{\frac{2kT_e(0)}{m_i}}. \tag{5.6}$$

The only unknown parameter in this equation is the cutoff velocity v_{cutoff} and so it can be determined from this equation. Once this has been done, the actual IV characteristic can be constructed. So far, the calculations dealt with an electrically isolated i. e. floating probe. Now, a potential V_{prb} shall be applied to the probe. This potential defines a new velocity w at which electrons can overcome the sheath. Since a floating probe is biased negatively, an applied potential will decrease the velocity necessary to overcome the total potential, thus giving w as

$$w = \sqrt{\frac{2}{m_e}\left(\frac{1}{2} m_e v_{\text{cutoff}}^2 - eV_{prb}\right)}. \tag{5.7}$$

The new electron current to the probe is given by

$$j_{prb}^{-}(V_{prb}) = e \int_{w}^{\infty} v_0 f(v_0) \mathrm{d}v_0. \tag{5.8}$$

The ion current remains unchanged and so net current is now drawn through the probe. This current is easily given by subtracting the electron current from the ion current,

$$j_{prb}(V_{prb}) = j_{prb}^{+} - j_{prb}^{-}(V_{prb}). \tag{5.9}$$

Finally, expression 5.9 is the actual IV characterstic of the target probe.

5.3.4 Choice of mean free path

In this section, the formula used to calculate the mean free path will be introduced. Following Stangeby's draft [9], expressions from the NRL Plasma formulary are used [17]. Let the index α refer to test electrons with velocity v_α and index β to the actual plasma particles into which the test particles are injected, with temperature $T_e(x)$ and density $n_e(x)$. Let $\chi^{\alpha/\beta} = \frac{m_\beta v_\alpha^2}{2kT_\alpha}$. [17] gives the various collision frequencies for fast electrons, that is to say when $\chi \gg 1$.

For stopping:

$$\nu_s = 7.7 \times 10^{-6} n \ln(\Lambda) \epsilon^{-3/2} \tag{5.10}$$

For perpendicular diffusion:

$$\nu_\perp = 7.7 \times 10^{-6} n \ln(\Lambda) \epsilon^{-3/2} \tag{5.11}$$

For parallel diffusion:

$$\nu_\parallel = 3.9 \times 10^{-6} n \ln(\Lambda) T \epsilon^{-5/2} \tag{5.12}$$

For energy:

$$\nu_\epsilon = 2\nu_s - \nu_\perp - \nu_\parallel \tag{5.13}$$

Where $\epsilon = \frac{1}{2e} m_e v^2$. In equations 5.10-5.13, $\nu[\mathrm{s}^{-1}], n[\mathrm{cm}^{-3}], T, \epsilon[\mathrm{eV}]$. According to [3], $\ln \Lambda = 17$ shall be used. From equations 5.10-5.13 the electron-electron collision mean free path can be expressed

$$\lambda_{\text{fast}}(\epsilon, T, n) = \frac{v_\epsilon}{\nu} = \frac{10^{12}\epsilon^2\sqrt{\frac{2e}{m_e}}}{n \ln \Lambda(7,7 - 3,9\frac{T_e}{\epsilon})} \tag{5.14}$$

For thermal electrons, $\epsilon = T$ and $\chi^{\alpha/\beta} = 1$, the thermal mean free path is used

$$\lambda_{\text{thermal}}(T, n) = 0,92 \times 10^{16}\frac{T^2}{n} \tag{5.15}$$

It is necessary to connect these two expressions in some way, so that the resulting mean free path is a continuos function of v. We have decided to use the following expression to calculate the mean free path:

$$\lambda(\epsilon, T, n) = \lambda_{\text{fast}} - (\lambda_{\text{fast}} - \lambda_{\text{thermal}}) \exp\big(-(1 - \frac{\epsilon}{2T_e})^2\big). \tag{5.16}$$

This expression provides smooth transition from the thermal mean free path to the super-thermal mean free path, Fig. 5.5. Electrons are regarded as thermal until two times the local T_e. Throughout the model, expression 5.15 is used for thermal and expression 5.16 for super-thermal electrons.

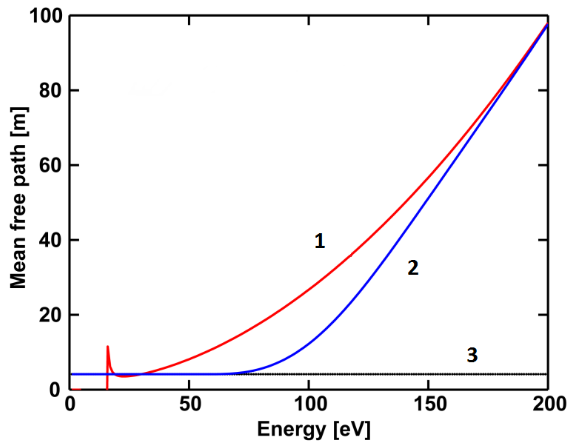

Figure 5.5: Mean free paths λ_{fast} (1), λ_{thermal} (3) and λ (2) of an electron with energy ϵ in a plasma at fixed temperature $T_e = 30$ eV and density $n_e = 2 \times 10^{19}\mathrm{m}^{-3}$.

5.3.5 Model results

In this section, results obtained from the simulation decribed in sections 5.3.2, 5.3.3 and 5.3.4 will be presented and interpreted for both TCV and JET input data. For TCV data, accord with the results in paper [5] will be shown.

TCV

It is expected that the electron velocity distribution function at the divertor target will be distorted, i. e. that the "tail" of the EVDF will be somewhat higher. Indeed, the model yields such EVDFs. The effect is most visible when a significant temperature gradient is present. This condition is met for the B profile, for example, section 5.3.1 and the corresponding EVDF is shown in Fig. 5.6. Similar more or less significant distortions can be observed for the rest of the profiles as well, depending on the temperature gradient. However, we are more interested in the IV characteristics, since the temperature is obtained from them. The IV characteristic is calculated from the distribution function as described in section 5.3.3 in a range of voltages pertinent to a real situation, from -100 V to 50 V. Next, the computed characteristic is fitted by equation 4.5 in order to obtain the electron temperature, just like as if it was experimental data. Assuming our model is correct, this is the temperature that a probe inserted in the given plasma is supposed to measure.

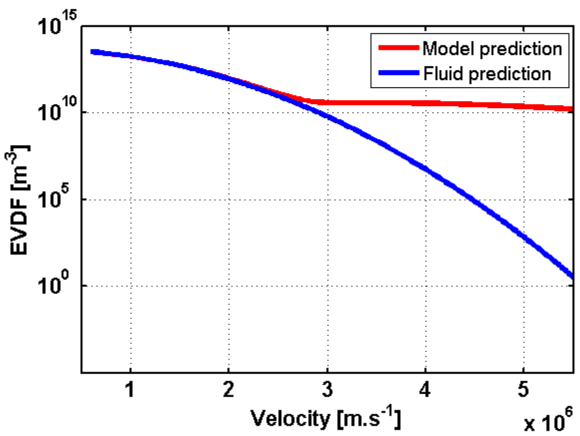

Figure 5.6: Distorted EVDF computed by the model (red) and Maxwellian EVDF (blue) at the inner divertor target. The distorted EVDF is calculated for profile B and the Maxwellian at the target is calculated for $T_e(0)$ and $n_e(0)$ from the B2-EIRENE fluid code. The y-axis uses logarithmic scaling due to poor visibility when using normal scaling.

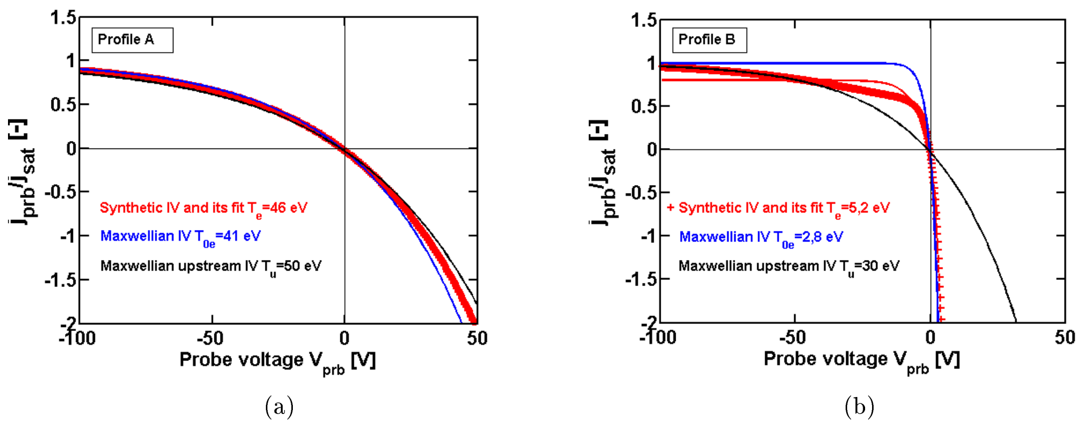

Figure 5.7: Computed IV characteristics at the target (red+) and their fits (red) compared to IV characteristics obtained for T_{0e} at the target (blue) and the maximum upstream temperature on the given profile T_u (black), both from the B2-EIRENE fluid code. Profiles A (a) with a less significant and B (b) with a significant temperature gradient are displayed. The characteristic is normalized to the ion saturation current.

In Fig. 5.7 two examples of IV characteristics for the inner divertor target for profiles A (less significant temperature gradient) and B (significant temperature gradient) are shown. In the case of the less significant temperature gradient, the computed EVDF and the corresponding IV characteristic the temperature T_e predicted by the model lies between the target T_0e and maximum upstream temperature T_u, Fig. 5.7(a). For the high temperature gradient in profile B, the computed EVDF and IV characteristic are more distorted and the computation yields T_e that is by a factor of ~ 2 higher than the target temperature predicted by the B2-EIRENE code, Fig. 5.7(b).

Fig. 5.8 compiles the main results of the model. By fitting the computed IV characteristics for each profile of the selected flux surface (a total of 8 parallel profiles) the temperatures (simulating Langmuir probe measurements) are obtained. These are plotted with respect to an upstream density, more precisely the density at the midplane. For comparison, the temperatures predicted by the B2-EIRENE fluid code for the target T_{0e} and the maximum upstream temperature on the profile, T_u are also plotted. The upstream location is simply chosen as the place of maximum temperature on the given profile.

For the inner divertor target, Fig. 5.8(a), Langmuir probes should predict overestimation of T_e measurements by factors in the range from ~ 1.5 to ~ 2 for intermediate midplane densities. On the other hand, for the outer divertor target, Fig. 5.8(b) probes seem to measure correct values of T_e, except for the low density cases.

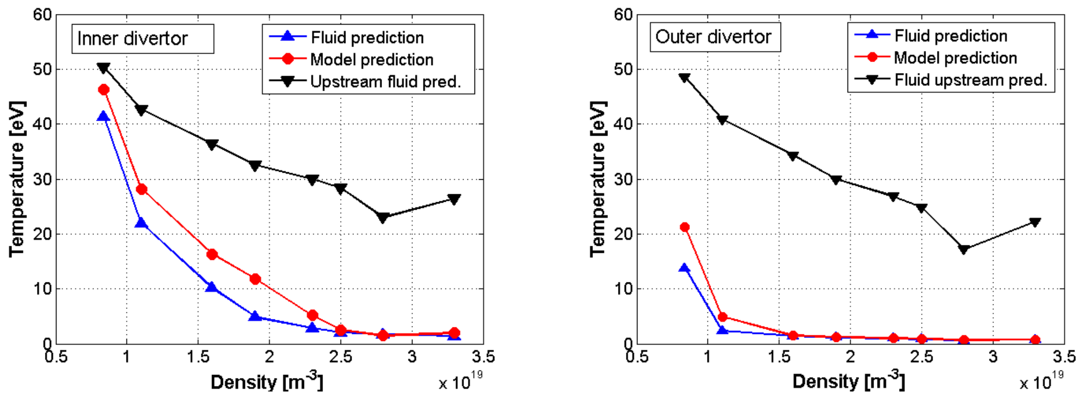

(a) (b)

Figure 5.8: Density scan of T_e predicted by the model compared to the temperature T_{0e} at the target and the maximum upstream temperature T_u, both from the B2-EIRENE generated parallel profiles.

The reason why inner target probes overestimate the temperature while outer probes do not seems to be clear. The standard TCV divertor geometry is poloidally assymetric, Fig. 5.2. The inner divertor leg is short which means that the distance from the target to the hot upstream regions is small. This gives rise significant temperature gradients. On the contrary, the outer divertor leg is long, flattening the temperature profile out, which can clearly be visible in Fig. 5.3. Electrons from the hot upstream regions have to travel a significantly greater distance to the outer target, making collisions more probable, hence distribution functions at the target are considerably less affected by these fast electrons.

Comparison with results in [5]

The results obtained by our model are in good accordance with the results in the paper of J. Horáček [5]. In the paper, outer divertor targets probes are expected to yield correct values of T_e, except for the low density cases, as in our model. For the inner divertor target, probes tend to overestimate the temperature for densities ranging form $10\times10^{-18}\mathrm{m}^{-3}$ to $20\times10^{-18}\mathrm{m}^{-3}$, which is in fair accordance with our predicition.

JET

For JET input data, the same simulation has been run. The simulated temperatures measured by Langmuir probes are obtained in the same manner as for TCV. At this point, only the density scan will be shown (scanning through the density at the stagnation point), Fig. 5.9 since it sums up the most important results of the model.

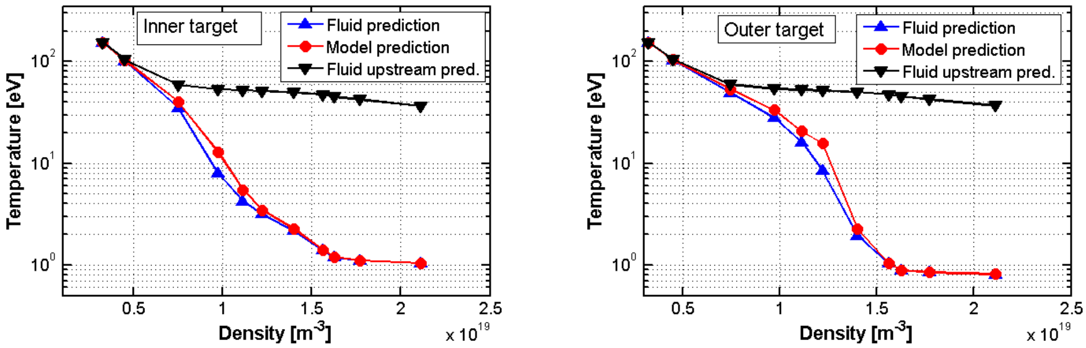

(a) (b)

Figure 5.9: Density scan of T_e predicted by the model compared to the temperature T_{0e} at the target and the maximum upstream temperature T_u, both from the EDGE-2D generated parallel profiles.

It can be seen that according to the model, JET divetor target Langmuir probes should measure the temperature correctly, both for the inner 5.9(a) and outer 5.9(b) target, except for intermediate densities. The JET divertor has an approximately symmetrical divertor geometry, hence making the profiles symmetrical, Fig. 5.4 at least compared to TCV, thus giving the same result for both the inner and outer divertor target probe.

Conclusion

Summary of the thesis

One of the objectives of the thesis was to give an overview of basic notions of plasma physics and the description of the main principles of the operation of tokamaks. These general concepts have been described in chapters 1 and 2 respectively, which are then widely used throughout the thesis.

Next, in chapter 3 the tokamak edge plasma was characterized, by defining the scrape-off layer and describing some basic transport phenomena in the SOL, as well as the function of limiters and divertors. The divertor SOL and transport ocurring in it was emphasized, since tokamaks having divertor configurations are our main interest in subsequent chapters. Chapter 4 gives an overview of the principal diagnostic methods used to obtain edge plasma parameters. Since diagnostics is an immense topic, only Langmuir probes were described thoroughly, as they are the point of interest of the final chapter. For the other diagnostic methods, only a summary view was given, describing the main principles of operation and their advantages, since a more detailed description would exceed the needs of this thesis.

Lastly, in chapter 5, the issue of Langmuir probe T_e overestimation at divertor targets was discussed. Two possible treatments have been described, computationally demanding PIC simulations and, in contrast, a simple kinetic model. This second approach comprises of the calculation of EVDFs at the divertor targets using parallel SOL profiles of T_e and n_e generated by fluid codes. Synthetic Langmuir probe IV characteristics are then computed from the EVDFs. The value of the electron temperature is determined from these synthetic IV characteristics in the same way as from experimental Langmuir probe IV data. Simulations have been run for both TCV (which was one of the objectives of the thesis) and JET input data. It is found that significant parallel temperature gradients distort the target EVDF, more precisely, they enhance the tail of the distribution, which afterwards leads to overestimation of Langmuir probe measurements. The main result for TCV is that for the inner divertor target, Langmuir probes should predict overestimation of T_e measurements by factors in the range from ~ 1.5 to ~ 2 for intermediate midplane densities. On the other hand, for the outer divertor target, probes seem to measure correct values of T_e, apart from the low density cases. These results turn out to be in good accordance with the results in paper [5], while this confirmation was also one of the goals of this thesis. For JET and the available input data, simulations predict that target probes should measure the T_e correctly, except for intermediate densities.

Future plans

Naturally, future perspectives concern the kinetic model used to simulate LP divertor target T_e measurements. The following developement is considered:

- Comparison of the model results with real experimental data from JET.
- Running simulations for a wider range of JET input data.
- Considering the fact that the fast electrons affect distribution functions all along the field lines, without giving rise to high computational requirements.
- Introducing a variable spatial step within the computation algorithm defined as a fraction of the local value of mean free path in order to get optimal spatial resolution all along the magnetic field line within the SOL.

List of acronyms

ASDEX Axially Symmetric Divertor Experiment

JET Joint European torus

EFDA European Fusion Development Agreement

ELM Edge Localized Mode

EURATOM European Atomic Energy Community

EVDF Electron Velocity Distribution Function

IR Infrared

LCFS Last Closed Flux Surface

LP Langmuir Probe

MAST Mega Amper Spherical Tokamak

PIC Parcticle in Cell

SOL Scrape-off layer

TCV Tokamak à Configuration Variable

TEXTOR Tokamak Experiment for Technology Oriented Research

Bibliography

[1] F. F. Chen, *Úvod do fyziky plazmatu*, Academia, Praha, 1984.

[2] J. Wesson, *Tokamaks*, Clarendon Press–Oxford University Press,2004.

[3] P. C. Stangeby *The plasma boundary of magnetic fusion devices*, IoP, 2000.

[4] I. H. Hutchinson, *Principles of plasma diagnostics*, Cambridge University Press, 2002.

[5] J. Horáček et al., *Predicted effects of parallel temperature gradients on the overestimation of TCV divertor target Langmuir probe Te measurements*, Journal of Nuclear Materials 313-316 (2003) 931-935.

[6] M. Hron, *Turbulence plazmatu na Tokamaku CASTOR*, disertační práce, MFF UK v Praze, 2002

[7] J. Brotánková, *Studium horkého plazmatu v experimentálních zařízeních typu tokamak*, disertační práce, MFF UK v Praze, 2009

[8] D. Tskhakaya et al., *Interpretation of divertor Langmuir probe measurements during ELMs at JET*, Journal of Nuclear Materials 415 (2011) 860-864.

[9] P. C. Stangeby, *Correction to Te values measured by a Langmuir probe allowing for weak collisionality of fast electrons*, in preparation

[10] A. Pochelon et al., *Energy confinement and MHD activity in shaped TCV plasmas with localized electron cyclotron heating*, Nuclear Fusion, Vol. 39, No. 11Y (1999) 1807-1818.

[11] S. V. Mirnov et al., *Experiments with lithium limiter on T-11M tokamak and applications of the lithium capillary-pore system in future fusion reactor devices*, Plasma Phys. Control. Fusion 48 (2006) 821–837.

[12] F. F. Chen ed R. H. Huddlestone and S. L. Leonard, *Plasma diagnostic techniques*, Academic, London, 1965.

[13] J. D. Swift, M. J. Schwarz, *Electric probes for plasma diagnostics*, Elsevier, London, 1969.

[14] G. F. Matthews et al., *Tokamak plasma diagnosis by electrical probes*, Plasma Phys. Control. Fusion 36 (1994) 1595.

[15] R. D. Monk et al., *Interpretation of ion flux and electron temperature profiles at the JET divertor target during high recycling and detached discharges*, Journal of Nuclear Materials 241–243 (1997) 396–401.

[16] G. Fussmann, U. Ditte, W. Eckstein, et al., *Divertor parameters and divertor operation in ASDEX*, Journal of Nuclear Materials 128-129 (1984) 350–358.

[17] J. D. Huba, *NRL plasma formulary*, Naval Research Laboratory, 2007.

[18] J. Wesson, *Effect of temperature gradient on plasma sheath*, Plasma Phys. Control. Fusion 37 (1995) 1459.

[19] D. Reiter, M. Baelmans and P. Börner, *The EIRENE and B2-EIRENE codes*, Fusion science and technology vol. 47 (2005) 172-186.

[20] J. Marki, *Infrared thermography of divertor ELM heat loads on TCV*, doctoral thesis, EPFL Lausanne, 2011